

Enhanced RNA-targeting CRISPR-Cas technology in zebrafish

Ismael Moreno-Sánchez^{1,2,3,#}, Luis Hernandez-Huertas^{1,2,#}, Daniel Nahon-Cano^{1,2,#}, Carlos Gomez-Marin^{1,2}, Pedro Manuel Martínez-García¹, Anthony J. Treichel⁴, Laura Tomas-Gallardo^{1,5}, Gabriel da Silva Pescador⁴, Gopal Kushawah⁴, Alejandro Díaz-Moscoso^{1,5,\$}, Alejandra Cano-Ruiz^{1,2}, John A. Walker II⁶, Manuel J. Muñoz^{1,2}, Kevin Holden⁶, Joan Galcerán^{3,7}, María Ángela Nieto^{3,7}, Ariel Bazzini^{4,8}, Miguel A. Moreno-Mateos^{1,2,*}

1 Andalusian Center for Developmental Biology (CABD), Pablo de Olavide University/CSIC/Junta de Andalucía, Ctra. Utrera Km.1, 41013, Seville, Spain.

2 Department of Molecular Biology and Biochemical Engineering, Pablo de Olavide University, Ctra. Utrera Km.1, 41013, Seville, Spain.

3 Instituto de Neurociencias (CSIC-UMH), Sant Joan d'Alacant, Alicante, Spain.

4 Stowers Institute for Medical Research, 1000 E 50th St, Kansas City, MO 64110, USA

5 Proteomics and Biochemistry Platform, Andalusian Center for Developmental Biology (CABD) Pablo de Olavide University/CSIC/Junta de Andalucía, Ctra. Utrera Km.1, 41013 Seville, Spain.

6 Synthego Corporation, Redwood City, CA, USA.

7 CIBERER, Centro de Investigación Biomédica en Red de Enfermedades Raras, ISCIII, Spain

8 Department of Molecular and Integrative Physiology, University of Kansas Medical Center, 3901 Rainbow Blvd, Kansas City, KS 66160, USA

\$ Current address: Instituto de Investigaciones Químicas (IIQ-CICIC), CSIC-US, Avda. Américo Vespucio 49, 41092 Seville, Spain.

These authors contributed equally to this work

*To whom correspondence should be addressed:

E-mail: mamormat@upo.es

Tel: +34 954349210

Fax: +34 954349376

Keywords: CRISPR-Cas, Cas13, Cas7-11, RNA-targeting, zebrafish, collateral activity

Running Title: Optimizing CRISPR-Cas RNA-targeting technology in zebrafish

39 **Summary**

40 CRISPR-Cas13 systems are widely used in basic and applied sciences.
41 However, its application has recently generated controversy due to collateral
42 activity in mammalian cells and mouse models. Moreover, its efficiency could be
43 improved *in vivo*. Here, we optimized transient formulations as ribonucleoprotein
44 complexes or mRNA-gRNA combinations to enhance the CRISPR-RfxCas13d
45 system in zebrafish. We i) used chemically modified gRNAs to allow more
46 penetrant loss-of-function phenotypes, ii) improved nuclear RNA-targeting, and
47 iii) compared different computational models and determined the most accurate
48 to predict gRNA activity *in vivo*. Furthermore, we demonstrated that transient
49 CRISPR-RfxCas13d can effectively deplete endogenous mRNAs in zebrafish
50 embryos without inducing collateral effects, except when targeting extremely
51 abundant and ectopic RNAs. Finally, we implemented alternative RNA-targeting
52 CRISPR-Cas systems with reduced or absent collateral activity. Altogether, these
53 findings contribute to CRISPR-Cas technology optimization for RNA targeting in
54 zebrafish through transient approaches and assist in the progression of *in vivo*
55 applications.

56

57 **Introduction**

58 RfxCas13d is a class 2/type VI CRISPR-Cas RNA endonuclease that
59 together with a guide RNA (gRNA) targets RNA by RNA-RNA hybridization. The
60 CRISPR-RfxCas13d system has been efficiently used to eliminate RNA and
61 therefore possesses extraordinary potential for biotechnology and biomedicine^{1–}
62 ⁶. We recently optimized this technology *in vivo* using ribonucleoprotein (RNP)
63 complexes or mRNA-gRNA delivery that allows effective, transient, and cytosolic
64 mRNA knockdown (KD) during vertebrate embryogenesis, including zebrafish,
65 medaka, killifish and mouse, among other vertebrate embryos^{7–15}. However,
66 through our continued work we have identified a set of limitations that need to be
67 addressed to further expand the *in vivo* capabilities of the CRISPR-RfxCas13d
68 system.

69 First, targeting nuclear RNAs or zygotically-expressed genes transcribed
70 after gastrulation is less efficient⁷. A second limitation is that a subset of *in vitro*
71 transcribed gRNAs, but not their chemically synthesized versions, can trigger
72 toxic effects during embryogenesis. Thirdly, as described in mammalian cells^{16–}
73 ¹⁹ and in other CRISPR-Cas systems both *in vivo* and *ex vivo*^{20–22}, on-target
74 gRNA activity is variable and can challenge the targeting efficiency⁷. Moreover,
75 CRISPR-RfxCas13d specificity has come under scrutiny lately due to the parallel
76 and recent discoveries of collateral activity in eukaryotic cells^{23–29}. Collateral
77 activity is a shared feature of all Cas13 family endonucleases and has been well
78 established in bacteria and *in vitro*^{30–32}. It is defined as the cleavage of non-target
79 RNAs that relies upon on-target gRNA recognition and stems from the three-
80 dimensional structure of the two HEPN (Higher Eukaryotes and Prokaryotes
81 Nucleotide-binding) nuclease domains in Cas13 family members. After the

82 activation and a conformational change of Cas13, the HEPN domains are
83 exposed on the outside of the protein and are able to cleave other accessible
84 RNA molecules^{33,34}. In eukaryotes, this phenomenon has been mainly observed
85 in *ex vivo* contexts such as mammalian or *Drosophila* cell cultures and/or when
86 gRNAs and RfxCas13d are highly expressed from constitutive promoters^{23–29}.
87 RfxCas13d collateral activity has yet to be characterized *in vivo* using transient
88 targeting approaches (the delivery of RNP or mRNA-gRNA formulations) or
89 assessed in the context of embryo development.

90 Here, we have enhanced RNA-targeting CRISPR-Cas technology *in vivo*
91 through different and compatible approaches using zebrafish embryos as a
92 model system. First, we show that chemically modified gRNAs, along with
93 *RfxCas13d* mRNA, significantly increase the loss-of-function phenotype
94 penetrance when targeting mRNA from genes with late expression during
95 development. Second, we have implemented an approach to select high-quality
96 *in vitro* transcribed gRNAs to avoid potential toxic effects *in vivo*. Third, we
97 optimize RfxCas13d nuclear targeting along zebrafish early development by
98 incorporating nuclear localization signals previously used to increase the activity
99 of DNA-targeting CRISPR-Cas systems. Fourth, we compare different
100 computational models recently developed in mammalian cell cultures^{17–19},
101 analyze their accuracy to predict the activity of 200 gRNAs delivered as RNP
102 complexes and define the most accurate approach for classifying CRISPR-
103 RfxCas13d efficiency *in vivo*. Fifth, we demonstrate that transient CRISPR-
104 RfxCas13d approaches can be used to deplete the vast majority of naturally
105 present mRNAs in zebrafish embryos without inducing collateral activity, although
106 this effect is triggered when targeting extremely abundant and ectopic mRNAs.

107 Finally, we evaluate and compare the on-target and collateral activity of other
108 RNA-targeting CRISPR-Cas systems, such as CRISPR-Cas7-11, CRISPR-
109 DjCas13d and a high-fidelity version of RfxCas13d, formulated as RNP
110 complexes. We demonstrate that CRISPR-Cas7-11 and specially CRISPR-
111 DjCas13d can efficiently eliminate mRNAs *in vivo* and with absent or lower
112 collateral effects than CRISPR-RfxCas13d, respectively when depleting highly
113 abundant and ectopic RNAs in zebrafish embryos. Overall, our work constitutes
114 a significant contribution towards better comprehension and enhancement of
115 transient CRISPR-Cas approaches to target RNA in zebrafish embryos that will
116 ultimately facilitate more effective integration of RNA-targeting CRISPR-Cas into
117 *in vivo* KD-based biotechnological and biomedical applications.

118

119 **Results**

120 **CRISPR-RfxCas13d guide RNA optimizations lead to straight-forward**
121 **and sustained targeting in zebrafish embryos.**

122 CRISPR-RfxCas13d has shown high activity when targeting maternally
123 provided and early transcribed mRNAs during vertebrate embryogenesis^{7-14,35}.
124 However, the system performed with lower efficiency when depleting genes
125 expressed later during development after 7-8 hours post-fertilization (hpf)⁷. Since
126 chemically modified gRNAs (cm-gRNAs) have been used to maintain the
127 efficiency of mRNA depletion in mammalian cell cultures³⁶, we hypothesized that
128 this could be used during zebrafish embryogenesis to sustain and increase RNA
129 targeting *in vivo*. We employed the most efficient chemical modification described
130 in *in vitro* approaches (cm-gRNAs, 2'-O-methyl analogs and 3'-phosphorothioate
131 internucleotide linkage in the last three nucleotides, Mendez-Mancilla et al.,

132 2022³⁶) combined with either mRNA or purified protein RfxCas13d (**Fig. 1A**). We
133 targeted different maternally-provided mRNAs and zygotically-transcribed
134 mRNAs in zebrafish embryos whose lack of function and phenotype penetrance
135 could be easily visualized and quantified^{7,8,37} (**Fig. 1B-E, Extended Data Fig. 1**).
136 For example, the KD of *nanog* mRNA leads to epiboly defects with a substantial
137 fraction of embryos at 30-50% epiboly at 6 hpf instead of germ ring or shield
138 stage. The KDs of *tbxta* (hereafter named as *no-tail*) and *noto* mRNAs cause a
139 reduction and/or the lack of the notochord and posterior part in the embryo (**Fig.**
140 **1C**). In addition, the KD of *rx3* impairs eye development, and the KDs of
141 *tyrosinase* (*tyr*), *slc45a2* (hereafter named as *albino*) and *slc24a5* (hereafter
142 named as *golden*) mRNAs produce a loss of pigmentation (**Fig. 1C, Extended**
143 **Data Fig. 1A**). While maternally-provided *nanog* mRNA was efficiently targeted
144 by RNP complexes without any improvement using cm-gRNAs (**Fig. 1D**), early
145 zygotically-expressed RNAs (*no-tail* and *noto*) KD experienced a subtle but still
146 significant increase in the phenotype penetrance (**Fig. 1D, Extended Data Fig.**
147 **1B**). Conversely, independently of the use of cm-gRNAs, RNP complexes were
148 much less active when targeting mRNAs from genes whose main expression
149 occurs later during development after 7-8 hpf (**Fig. 1B, Extended Data Fig. 1B**).
150 Notably, the combination of *RfxCas13d* mRNA and cm-gRNA showed a superior
151 efficiency eliminating these mRNAs with a more penetrant phenotype and robust
152 targeting (**Fig. 1E, Extended Data Fig. 1C-D**). Altogether, these results
153 demonstrate that cm-gRNAs increase the activity of CRISPR-RfxCas13d on
154 transcripts from genes expressed later during zebrafish embryogenesis and
155 validate the use of cm-gRNA to deplete RNA *in vivo*. Additionally, we tested
156 whether longer spacers (30 nucleotides, nt) might slightly boost RNA depletion *in*

157 *vivo* by CRISPR-RfxCas13d as it was previously described in mammalian cell
158 cultures¹⁶. However, either 23 or 30 nt gRNAs led to a similar efficiency targeting
159 maternal or zygotically expressed mRNAs with both RfxCas13d mRNA or protein
160 (**Extended Data Fig. 2**).

161 In all previous experiments (**Fig. 1 and Extended Data Fig. 1 and 2**), we
162 employed chemically synthesized and commercially available gRNAs (see
163 Methods). Alternatively, efficient and specific gRNAs can be produced through
164 oligo-annealing and fill-in PCR, followed by *in vitro* transcription (hereafter: IVTed
165 gRNAs)^{7,8}. Nevertheless, employing IVTed gRNAs we have occasionally
166 observed toxic effects in zebrafish embryos. For example, when targeting *si:dkey-*
167 *93m18.4* mRNA, a lowly expressed transcript, with three individual IVTed gRNAs,
168 we detected three distinct phenotypes when injected with RfxCas13d protein.
169 While gRNA-1 had no effect during embryogenesis, gRNA-2 showed early
170 embryogenesis delay, and gRNA-3 was lethal with previous developmental
171 defects even by 2 hpf (**Fig. 2A, Extended Data Fig. 3A**). Conversely, targeting
172 *si:dkey-93m18.4* mRNA with any of these three gRNAs showed comparably
173 strong (>90%) KD at 4 hpf (**Fig. 2B**). We next wondered whether this toxic effect
174 stemmed from *in vitro* transcription synthesis or was a direct result of gRNA
175 sequence. To address this, we used chemically synthesized gRNA-1 and gRNA-
176 3 targeting *si:dkey-93m18.4* mRNA. Injection of chemically synthesized gRNA-1
177 produced no developmental effects, as expected. In contrast to the lethality
178 observed with IVTed gRNA-3, embryos injected with chemically synthesized
179 gRNA-3 exhibited normal development (**Fig. 2A, Extended Data Fig. 3A**).
180 Critically, RfxCas13d with chemically synthesized gRNAs achieved similar
181 *si:dkey-93m18.4* knockdown to their IVTed counterparts (**Fig. 2B**). Taken

182 together, this data demonstrates that a subset of RfxCas13d gRNAs can have
183 toxic effects when produced by *in vitro* transcription.

184 One of the molecular outcomes from these toxic effects was that, beyond
185 the expected 18S and 28S ribosomal RNA (rRNA) observed in an RNA integrity
186 analysis, we detected two prominent RNA species (**Fig. 2C, Extended Data Fig.**
187 **3B**) in *si:dkey-93m18.4* KDs consistently of ~1000 and ~2500 nucleotides (nt) in
188 length and associated with developmental effects. We employed these two 28S
189 rRNA cleavage species and their positions to ratiometrically quantify the integrity
190 of the 28S rRNA. Controls and *si:dkey-93m18.4* KDs without developmental
191 effects exhibited similar 28S integrity (**Fig. 2D-E**) whereas KDs with IVTed gRNA-
192 2 and gRNA-3 showed significant decreases in 28S integrity that scale with both
193 phenotype onset and severity (**Fig. 2A, C-E, Extended Data Fig. 3A-B**).

194 Correspondingly, we observed similar results when we targeted *brd4*
195 mRNA using an IVTed or a chemically synthesized gRNA, both inducing a
196 significant reduction of transcript levels (**Fig. 2F-G**). *Brd4* mRNA knockdown
197 causes epiboly defects⁷ that were recapitulated by the chemically synthesized
198 gRNA (**Fig. 2F**). However, the IVTed gRNA triggered a severe early
199 embryogenesis lethality associated with a 28S rRNA fragmentation (**Fig. 2F and**
200 **H and Extended Data Fig. 3B**).

201 Furthermore, we developed a simple *in vitro* rRNA integrity assay method
202 to screen for IVTed gRNAs without a 28S rRNA cleavage effect associated with
203 toxicity. We combined RfxCas13d protein, and/or gRNA with zebrafish total RNA
204 and examined the total RNA through electrophoresis (**Extended Data Fig. 3C**).
205 For example, in *si:dkey-93m18.4* KDs we observed that neither RfxCas13d alone
206 nor gRNA-1 or chemically synthesized gRNAs (1 and 3) as well as gRNAs alone

207 (**Extended Data Fig. 3D**) had any substantial effect on the rRNA integrity in this
208 assay. In contrast, RfxCas13d with IVT^d gRNA-2 and gRNA-3 triggered rRNA
209 cleavage *in vitro* (**Extended Data Fig. 3D**), which was more severe than that
210 observed in total RNA from injected embryos (**Extended Data Fig. 3B**).

211 Altogether, these data demonstrated that some IVT^d gRNAs for
212 RfxCas13d may trigger 28S rRNA fragmentation *in vitro* and *in vivo* that is
213 associated with severe defects during embryogenesis and toxicity. Importantly,
214 these toxic effects can be overcome by i) using chemically synthesized gRNAs
215 or ii) pre-screening IVT^d gRNAs with our *in vitro* rRNA integrity assay.

216

217 **Enhancing nuclear RNA depletion by CRISPR-RfxCas13d in zebrafish
218 embryos.**

219 Efficient nuclear RNA targeting can be crucial to eliminate RNAs located
220 in this cellular compartment, such as long non-coding RNAs or primary
221 microRNAs^{38–40}. However, our optimized approach triggers mRNA KD in the
222 cytosol. Indeed, a version of RfxCas13d with nuclear localization signals (NLS,
223 RfxCas13d-NLS) was much less active in zebrafish embryos⁷ in contrast to what
224 it was observed in mammalian cell cultures when RfxCas13d targets the nascent
225 mRNA⁴¹. We hypothesized that the optimization of NLS could improve the
226 efficacy of nuclear RNA elimination mediated by RfxCas13d in zebrafish
227 embryos. We tested 4 NLS formulations that have shown to increase nuclear
228 targeting effectiveness with CRISPR-Cas systems with DNA endonuclease
229 activity^{42–45}. All NLS versions were innocuous during early zebrafish development
230 when fused to RfxCas13d (**Extended Data Fig. 4**). We observed that 2 NLS
231 (SV40-Nucleoplasmin long NLS) at the carboxy-terminus⁴² of RfxCas13d

232 (RfxCas13d-2C-NLS) significantly caused the highest phenotype penetrance
233 observed at 48 hpf targeting the primary and nuclear transcript of miR-430 (pri-
234 miR-430) (**Fig. 3A-B**), a microRNA involved in early development regulation that
235 eliminate hundreds of mRNAs during the first hours of development⁴⁶⁻⁴⁸. Indeed,
236 this pri-miR-430 targeting induced by RfxCas13d-2C-NLS, specifically triggered
237 a global stabilization of a subset of mRNAs (n=203) whose degradation was more
238 strictly dependent on miR-430^{49,50} (**Fig. 3C**) without any substantial alteration of
239 other maternal mRNA decay programs depending on other maternally-provided
240 or zygotically-expressed factors⁵⁰. Notably, despite the intrinsic mosaicism of the
241 microinjection, pri-miR-430 KD phenotype at 48h hpf was partially rescued by a
242 mature version of miR-430 (**Fig. 3D**), strongly suggesting that observed
243 developmental defects were specifically caused by the miR-430 loss-of-function.
244 In addition, the optimized RfxCas13d-2C-NLS also triggered efficient and
245 significant KD of a small nuclear RNA, *u4atac* snRNA⁵¹, that was not depleted by
246 cytosolic RfxCas13d or our previous RfxCas13d-NLS⁷ (**Fig. 3E**).

247 Altogether, our results demonstrate that CRISPR-RfxCas13d-2C-NLS
248 system used as a mRNA-gRNA formulation efficiently depletes nuclear RNAs in
249 zebrafish embryos.

250

251 **RNAtargeting, an ex vivo-based computational model, can**
252 **moderately predict CRISPR-RfxCas13d activity *in vivo*.**

253 Several computational models have been recently developed to predict
254 CRISPR-RfxCas13d activity¹⁶⁻¹⁹. These models were based on data where
255 RfxCas13d and gRNAs were expressed from constitutive promoters in
256 mammalian cell cultures¹⁶⁻¹⁹. However, *in vivo* approaches frequently imply the

257 delivery of a purified RfxCas13d protein or RfxCas13d mRNA and chemically
258 synthesized or *in vitro* transcribed gRNAs. To examine whether computational
259 models based on cell culture data were able to accurately predict CRISPR-
260 RfxCas13d activity *in vivo*, we measured the efficiency of approximately 200
261 gRNAs in zebrafish embryos using our optimized and transient approach based
262 on RNP complexes. First, to define the maximal number of gRNAs that could be
263 used in zebrafish embryos allowing a successful detection of highly active
264 gRNAs, we co-injected 10 and 25 gRNAs as optimal and suboptimal targeting
265 conditions (100 pg and 40 pg of gRNA per embryo, respectively) (**Extended Data**
266 **Fig. 5A-B**). Next, we generated gRNA quintiles (q) based on their activity and
267 observed that up to 25 gRNAs injected together allowed us to detect highly
268 efficient gRNAs (q4 and q5, respectively) previously identified in optimal
269 conditions (**Extended Data Fig. 5**, fold change > 3.5, q4 and q5). Consequently,
270 we injected 8 independent combinations (gRNA set 1 to 8) of 25 gRNAs to KD 75
271 mRNAs (2-3 gRNAs per transcript) with high-moderate and stable levels between
272 1 and 4 hpf, where most of the targeting likely occurs (**Fig. 4A, Extended Data**
273 **Fig. 5C**). Then, we performed a RNA-seq analysis of each gRNA set at 4 hpf
274 (**Extended Data Fig. 6A-B**) and analyzed the efficiency of those gRNAs (n=191)
275 whose activity could be predicted by the most recent and updated computational
276 CRISPR-RfxCas13d models based on the activity of hundreds of thousands
277 constitutively expressed gRNAs in mammalian cell culture¹⁷⁻¹⁹ (**Fig. 4A** and see
278 Methods for details). Among the assessed models, RNAtargeting¹⁹ was the most
279 accurate classifying CRISPR-RfxCas13d RNP complexes activity in zebrafish
280 embryos (**Fig. 4B, Extended Data Fig. 6C**). Indeed, RNAtargeting was able to
281 classify 5 out of 8 set of gRNAs with a similar or even more accuracy than what

282 was calculated for an independent *ex vivo* data used as control (Cell culture data,
283 Pearson's correlation coefficient R> 0.38, **Fig. 4B**). Furthermore, RNAtargeting
284 was the most efficient computational model distinguishing highly (top 5) from
285 poorly (bottom 5) active gRNAs per set (**Fig. 4C-E**). These results suggest that
286 RNAtargeting is the most useful current tool to select competent gRNAs.
287 Nevertheless, RNAtargeting was less accurate at predicting CRISPR-RfxCas13d
288 RNP activity in 3 out 8 sets, especially in one of them where there was not a
289 positive correlation between the predicted scores and *in vivo* activity (**Fig. 4B**;
290 gRNA set 7, Pearson's correlation coefficient R= -0.05). Together, our results
291 validate the use of RNAtargeting to moderately classify CRISPR-RfxCas13d
292 activity delivered *in vivo* as RNP complexes.

293

294 **Minimal collateral activity targeting endogenous mRNAs by CRISPR-
295 RfxCas13d**

296 The recently described collateral activity triggered by CRISPR-RfxCas13d
297 induces different molecular outcomes that can be used as hallmarks of this effect.
298 The main consequence of this effect is the uncontrolled elimination of RNAs after
299 the specific and initial targeting of both exogenous and endogenous transcripts^{25–}
300 ²⁹. Besides, CRISPR-RfxCas13d-induced collateral activity is most severe when
301 targeting highly expressed genes and ultimately causes cell toxicity, a decrease
302 in cell proliferation^{25,26,29} and the cleavage of the 28S rRNA subunit^{26,29}. First, and
303 despite that we did not clearly detect any of these effects when previously using
304 our optimized RNP or mRNA-gRNA injections targeting endogenous or ectopic
305 mRNAs^{7,8,14}, we sought to investigate the collateral activity when CRISPR-
306 RfxCas13d system targeted a highly concentrated reporter (green fluorescent

307 protein, GFP) mRNA injected in one-cell stage zebrafish embryos. We observed
308 that, for different amounts (from 10 to 100 pg per embryo) of target, CRISPR-
309 RfxCas13d efficiently depleted both mRNA and GFP protein (**Fig. 5A-D**). Notably,
310 embryos injected with more than 50 pg of *gfp* mRNA experienced epiboly defects
311 at 6 hpf (**Fig. 5E**, 30-50% epiboly) when using CRISPR-RfxCas13d as a mRNA-
312 gRNA complex. This effect was more severe when using RNP complexes and,
313 indeed, the KD of 20 or more pg of *gfp* mRNA triggered not only embryogenesis
314 deficiencies but also an arrest during early development and death with the
315 highest concentrations (100 pg per embryo caused a massive embryo death, data
316 not shown) (**Fig. 5F**). Moreover, we observed a cleavage of the 28S rRNA subunit
317 in zebrafish embryos under these conditions correlating with a reduced RNA
318 integrative number (RIN) (**Extended Data Fig. 7A-C**). Interestingly, even with the
319 lowest concentration of *gfp* mRNA (10 pg per embryo), where no developmental
320 delay was noticed upon KD, a notable 28S rRNA fragmentation could be
321 visualized. This result suggests that RNA integrity assay was highly sensitive to
322 detect the collateral activity induced by CRISPR-RfxCas13d (**Extended Data**
323 **Fig. 7A-B**). Further, when a red fluorescent protein (DsRed) mRNA was co-
324 injected together with CRISPR-RfxCas13d RNP targeting *gfp* mRNA, the
325 fluorescence of both reporters decreased (except for the lowest concentration of
326 *gfp* mRNA), although the developmental and molecular (28S rRNA
327 fragmentation) effects were less severe (**Extended Data Fig. 7D-G**). This could
328 likely be due to a buffer capacity from the *dsred* mRNA that, at high concentration,
329 could partially alleviate the consequences of the collateral activity. To further
330 understand the molecular consequences of the collateral activity during zebrafish
331 embryogenesis, we performed a transcriptome analysis. We observed a global

332 deregulation specifically when targeting an extremely abundant amount of *gfp*
333 mRNA (50 pg/embryo), with 1145 downregulated and 1377 upregulated genes,
334 (**Fig. 5G, Extended Data Fig. 7H**) that correlates with the developmental defects
335 and 28S rRNA fragmentation previously observed. Together, our results
336 demonstrate that RfxCas13d can trigger collateral activity upon the targeting of
337 highly abundant reporter mRNAs.

338 Next, we sought to analyze whether the collateral activity could be
339 detected when targeting endogenous mRNAs. We selected 3 maternally
340 provided transcripts in zebrafish embryos, all above the top 25 most abundant
341 mRNAs among the polyadenylated mRNAs during the first 6 hpf (**Extended Data**
342 **Fig. 8A**). When we targeted these mRNAs, we did not observe any
343 developmental defect despite triggering a significant depletion of these
344 endogenous mRNAs (between 75-95% mRNA reduction) (**Fig. 5H-I**). In addition,
345 we did not notice any collateral downregulation of GFP fluorescence from its
346 mRNA that was co-injected together with RNP complexes targeting these
347 endogenous mRNAs (**Extended Data Fig. 8B**). Interestingly, for the depleted
348 endogenous targets, we detected a weak 28S rRNA fragmentation that was much
349 less prominent than observed when targeting the lowest tested amount of *gfp*
350 mRNA (**Extended Data Fig. 7A-B and 8C**). Nevertheless, this 28S rRNA
351 fragmentation was still significant when rRNA 28S integrity ratio was analyzed
352 (**Fig. 2D and Extended Data Fig. 8D**). This result indicates a minor collateral
353 effect yet without any significant physiological consequence (**Fig. 5H**). Notably,
354 we observed similar results when these endogenous mRNAs were targeted by
355 CRISPR-RfxCas13d RNP complexes without *gfp* mRNA, suggesting that the
356 presence of this transcript did not influence or buffer the collateral effects in these

357 conditions (**Extended Data Fig. 8E-G**). Altogether, our results suggest that the
358 collateral activity from CRISPR-RfxCas13d is minimal and without a physiological
359 relevance even targeting highly abundant mRNAs during zebrafish
360 embryogenesis, but it can be triggered when extremely expressed and ectopic
361 mRNAs such as injected reporters are eliminated.

362

363 **Implementation of alternative CRISPR-Cas systems for transient**
364 **RNA-targeting *in vivo*.**

365 Although minimal when targeting endogenous mRNAs, the collateral
366 activity induced by RfxCas13d can still be an issue under certain circumstances
367 *in vivo*. Additionally, the use of RNA-targeting CRISPR-Cas technology as a
368 potential therapeutic application driven by transient approaches needs to ensure
369 a biosafety method where the collateral activity should be minimized or totally
370 absent. Thus, we sought to optimize other RNA-targeting CRISPR-Cas systems
371 *in vivo* that have recently shown a reduced or lack of collateral activity while
372 preserving high on-target efficacy when expressed from constitutive and strong
373 promoters: a high-fidelity version of CRISPR-RfxCas13d (Hf-RfxCas13d²⁵),
374 CRISPR-Cas7-11⁵² and CRISPR-DjCas13d¹⁹. First, we purified these Cas
375 proteins and tested them in zebrafish embryos. None of the protein showed a
376 substantial toxicity when injected alone (**Extended Data Fig. 9A**). Second, we
377 used these Cas proteins to target *no-tail* and *nanog* using 1 and 3 gRNAs per
378 mRNA, respectively. To analyze the efficiency of these systems compared with
379 CRISPR-RfxCas13d, we quantified the phenotype penetrance upon the KD of
380 *nanog* and *no-tail*. While DjCas13d induced a similar phenotype penetrance to
381 RfxCas13d, Hf-RfxCas13d was much less efficient not only when injected as

382 purified protein but also as mRNA (**Fig. 6A-C, Extended Data Fig. 9B-D**),
383 suggesting that this endonuclease, transiently delivered as RNP or mRNA-gRNA
384 complexes, is not highly competent to target mRNA *in vivo*. Further, CRISPR-
385 Cas7-11 recapitulated the expected phenotype from the lack-of-function of *nanog*
386 and *no-tail* with a slightly lower activity than CRISPR-Cas13d systems (**Fig. 6A-**
387 **C**). Third, we quantified the mRNA levels of *nanog*, *no-tail* and three highly
388 abundant endogenous transcripts (*hnrrnpa0l*, *hmga1a*, *hspa8*) formerly analyzed
389 using RfxCas13d (**Fig. 5H-I, Extended Data Fig. 8E-F**) and targeted now by Hf-
390 RfxCas13d, DjCas13d and Cas7-11. Our results validated our previous data
391 based on phenotype analysis (**Fig. 6A-C, Extended Data Fig. 9B-C**), and
392 confirmed that Hf-RfxCas13d showed the lowest efficacy *in vivo* (42.2% average
393 depletion) followed by Cas7-11 (60.1%) and DjCas13d (83.2%) that triggered an
394 efficient mRNA depletion comparable to RfxCas13d activity (80.1%) (**Fig. 6D-I**).
395 Next, we investigated whether DjCas13d and Cas7-11 showed collateral activity
396 in zebrafish embryos using our previously defined conditions that allow us to
397 measure this effect employing reporter mRNAs. When targeting injected *gfp*
398 mRNA, DjCas13d displayed less severe developmental defects than RfxCas13d.
399 This toxicity increased with the concentration of the target, in agreement with
400 what was observed previously for RfxCas13d in *ex vivo* and *in vivo* conditions^{25,26}
401 (**Fig. 6J-K, Extended Data Fig. 9E, G, I**). Interestingly, and despite the
402 developmental defects, the fragmentation of the 28S rRNA was not observed
403 (**Extended Data Fig. 9K**) but we detected a non-specific downregulation of
404 DsRed fluorescence when its mRNA was co-injected with high amounts of *gfp*
405 mRNA (**Extended Data Fig. 10A-C**). Notably, and as observed for RfxCas13d,
406 the developmental phenotype triggered by *gfp* mRNA KD was mitigated when

407 *dsred* mRNA was co-injected, suggesting a buffer effect that alleviates this
408 alteration during embryogenesis (**Fig. 6J, Extended Data Fig. 10A-C**). In
409 contrast, Cas7-11 did not show neither developmental defects nor 28S rRNA
410 cleavage when targeting *gfp* mRNA (**Fig. 6J-K, Extended Data Fig. 9F, H, J, L**).
411 We also measured DsRed fluorescence when its mRNA was co-injected together
412 with Cas7-11 RNP and *gfp* mRNA and we did not detect any significant decrease
413 in protein activity (**Extended Data Fig. 10D-F**).

414 In addition, we performed a whole transcriptomic analysis and observed
415 that while the *gfp* mRNA depletion was highly efficient using either RfxCas13d or
416 DjCas13d (62.68 and 145.01 *gfp* mRNA fold-change, respectively), the
417 transcriptomic deregulation was strongly reduced when employing DjCas13d (a
418 98% and 91.4% reduction in number of downregulated and upregulated mRNAs
419 in the most extreme condition: 50 pg *gfp* mRNA, **Fig. 6L, Extended Data Fig.**
420 **11**). Conversely, *gfp* mRNA depletion mediated by Cas7-11 did not trigger any
421 significant transcriptomic alteration (**Fig. 6L**), but as previously shown (**Fig. 6E-**
422 **I**), the efficiency of this endonuclease was lower than DjCas13d or RfxCas13d
423 (Cas7-11: 4.26 *gfp* mRNA fold-change, **Extended Data Fig. 11**). Together, our
424 results i) reaffirm that CRISPR-RfxCas13d is an efficient and robust approach to
425 target endogenous mRNA in zebrafish embryos and ii) demonstrate that
426 CRISPR-Cas7-11 and CRISPR-DjCas13d RNP can be used as alternative
427 systems exhibiting a slightly lower or similar on-target activity than CRISPR-
428 RfxCas13d and showing a total absence or reduced collateral effects when
429 targeting extremely abundant ectopic RNAs, respectively.

430

431

432 **Discussion**

433 Our optimized CRISPR-RfxCas13d system has shown a high level of
434 efficiency and specificity targeting maternal and early-zygotically transcribed
435 genes in zebrafish and other vertebrate embryos^{7–14}. Here, we have further
436 enhanced CRISPR-Cas RNA-targeting *in vivo* using RNP and mRNA-gRNA
437 formulations in zebrafish as a vertebrate model through different and
438 complementary approaches. First, we have found that chemically modified
439 gRNAs (cm-gRNAs) are able to maintain and increase the activity of CRISPR-
440 RfxCas13d as described in human cells³⁶ specially modulating the expression of
441 genes zygotically-transcribed later during development where RNP complexes
442 were less efficient. Although DNA-targeting CRISPR-Cas systems can generate
443 null alleles, this can obscure gene activities that can be compensated through
444 transcriptional adaptation or only detected with a limited gene expression
445 reduction^{53–55}. RfxCas13d together with cm-gRNAs allow to titrate mRNA levels
446 of the target that can be an alternative for these scenarios. Indeed, our optimized
447 CRISPR-RfxCas13d system using cm-gRNAs could contribute to widen the
448 applications of combining transient perturbations with single-cell transcriptomics.
449 This approach could allow to simultaneously associate the level of target
450 depletion with a transcriptomic output at single cell level extending the use of this
451 technology recently integrated with zebrafish crisprants or F0 mutant embryos
452 targeted by DNA-targeting CRISPR-Cas approaches⁵⁶. Notably, cm-gRNAs have
453 also been recently shown to be useful in zebrafish RNA imaging, expanding their
454 applications *in vivo*⁵⁷.

455 Second, we have increased nuclear RNA targeting throughout zebrafish
456 embryogenesis using an enhanced NLS formulation. Indeed, we efficiently

457 eliminated nuclear non-coding RNAs such as pri-miR-430 or a snRNA (*u4atac*).
458 The incomplete maturity of the nuclear pore complexes during early zebrafish
459 development that impair nuclear protein import⁵⁸ can affect nuclear DNA or RNA
460 targeting and our results suggest that this may be partially circumvented with an
461 optimized NLS. Notably, this NLS was previously applied to enhance DNA
462 targeting through Cas12a, not only in zebrafish embryos but also in mammalian
463 cells⁴², suggesting that it could be used to improve the nuclear RNA targeting of
464 other CRISPR-Cas systems in different *in vivo* and *ex vivo* models.

465 Third, we have demonstrated that CRISPR-RfxCas13d RNP activity *in vivo*
466 can be classified, and highly active gRNAs can be predicted by RNAtargeting, a
467 computational model based on mammalian cell culture data, yet with a lower
468 accuracy than shown for approaches with a constitutive expression of both
469 RfxCas13d and gRNA¹⁹ (**Fig 4B**). However, RNAtargeting is based on the activity
470 from 127000 gRNAs whose spacers were 30 nt long¹⁹. Although we have shown
471 that RNP activity *in vivo* is similar employing gRNAs with either short (23 nt) or
472 long (30 nt) spacers (**Extended Data Fig. 2**) and we have precisely adapted
473 RNAtargeting to predict our data set based on short spacers (**Fig 4B and see**
474 **Methods for details**), we can not rule out that the prediction of CRISPR-
475 RfxCas13d RNP activity *in vivo* could be improved when using long spacers.
476 Nevertheless, it has been previously reported that computational models
477 predicting CRISPR-Cas DNA-targeting activity notably differ depending on the
478 employed method. Thus, CRISPR-SpCas9 efficiency prediction models depend
479 on whether the gRNA is constitutively transcribed from a U6 promoter or
480 generated *in vitro*⁵⁹. Considering this and previous CRISPR-Cas activity
481 analysis^{20,59}, we speculate that a computational model based on RNP complexes

482 or mRNA-gRNA formulations could outperform the predictive power of
483 RNA targeting for CRISPR-RfxCas13d activity in zebrafish embryos and enhance
484 the accuracy when selecting highly active gRNAs *in vivo*. Beyond zebrafish
485 embryos, this model could be additionally applied for other biotechnological or
486 biomedical applications where these transient approaches could be used.

487 Fourth, we have characterized the collateral activity of CRISPR-
488 RfxCas13d in zebrafish embryos previously detected *in vitro* and *in vivo*^{23,25-29}.
489 We have now analyzed this effect in different molecular and physiological
490 contexts by employing transient RNA-targeting approaches such as RNP
491 complexes and RfxCas13d mRNA-gRNA formulations during early zebrafish
492 embryogenesis. Importantly, we confirmed that CRISPR-RfxCas13d is very
493 specific, and relevant collateral effects only occur when targeting extremely
494 abundant ectopic RNAs such as *gfp* mRNA. We found that the toxicity and the
495 physiological consequences of the collateral activity increased with the
496 concentration of the *gfp* transcript as described in mammalian cells mRNA^{25,26}
497 (*i.e.* 50 pg of *gfp* mRNA injected per embryo: 10000 TPM at 6 hpf, **Fig. 5E-G**).
498 Interestingly, despite the depletion of lower amounts of *gfp* mRNA (*i.e.* 10 pg per
499 embryo) caused a deregulation of the transcriptome and 28S rRNA
500 fragmentation, it did not induce a developmental defect. Indeed, targeting highly
501 abundant endogenous mRNAs triggered an even fainter 28S rRNA fragmentation
502 and did not generate an early embryogenesis alteration either (**Fig. 5H-I**,
503 **Extended Data Fig. 8C-D**). These findings suggest that ectopic RNAs can elicit
504 much more collateral and toxic effects *in vivo* than endogenous transcripts as
505 reported in mammalian cell cultures^{25,28}. Nevertheless, when extremely abundant
506 mRNAs are targeted by CRISPR-RfxCas13d RNP complexes in zebrafish

507 embryos, a simple *in vitro* 28S rRNA cleavage assay can be used to detect even
508 a weak collateral activity without developmental defects (**Extended Data Fig. 8C-**
509 **D**). In addition, a subset of *in vitro* transcribed gRNAs can trigger toxicity *in vivo*
510 that resembles collateral activity consequences observed when targeting
511 extremely abundant and ectopic mRNA. Whether this effect is certainly CRISPR-
512 RfxCas13d collateral activity remains to be clarified. However, this deleterious
513 response is specifically due to the *in vitro* transcription reaction since the same
514 gRNA when chemically synthesized did not generate any toxic effect while
515 maintaining a similar efficiency of mRNA depletion (**Fig. 2, Extended Data Fig.**
516 **3**). In contrast, chemically synthesized are more expensive than *in vitro*
517 transcribed gRNAs and their use can be limited due to the higher cost. Therefore,
518 in case of using *in vitro* transcribed gRNAs we have optimized a fast and straight-
519 forward *in vitro* assay to determine their potential toxic activity that allows to
520 screen for reliable gRNAs to be used *in vivo*. Why this subset of gRNAs induces
521 toxicity during zebrafish embryogenesis depending on whether they are
522 chemically synthesized or *in vitro* transcribed remains to be determined.

523 Finally, and as an *in vivo* alternative to RfxCas13d specially when targeting
524 extremely abundant transcripts, we have compared the activity of three RNA-
525 targeting CRISPR-Cas systems that showed less or absent collateral activity
526 when gRNAs and Cas were expressed from strong and constitutive
527 promoters^{19,25,52}. While Hf-RfxCas13d²⁵ exhibited low targeting activity (**Fig. 6A-**
528 **C and I, Extended Data Fig. 9B-D**), Cas7-11⁵² and DjCas13d¹⁹ were more
529 active, the latter showing an efficiency comparable to RfxCas13d (**Fig. 6A-C and**
530 **I**). Interestingly, a recent preprint pointed out that Hf-RfxCas13d activity was
531 inferior than initially described likely due to the lower level of expression of this

532 endonuclease used in this report⁶⁰. Further, this preprint revealed that the
533 concentration of CRISPR-RfxCas13d reagents in mammalian cell culture is
534 crucial to induce collateral activity⁶⁰. Strikingly, we recapitulated these results
535 using a limited amount of CRISPR-RfxCas13d RNP or mRNA-gRNA complexes
536 that show an absence of toxic effects *in vivo* when targeting endogenous
537 mRNAs¹⁴ (**Fig. 5H and I, Extended Data 8**). Nevertheless, DjCas13d and Cas7-
538 11 reduced or abolish, respectively, the developmental defects during zebrafish
539 embryogenesis and the transcriptomic deregulation observed when RfxCas13d
540 was used to eliminate ectopic and highly expressed RNAs (**Fig. 6J-L, Extended**
541 **Data Fig. 9E-L and Extended Data Fig. 11**). However, DjCas13d did not totally
542 lack the collateral activity when targeting extremely abundant and ectopic mRNAs
543 inducing a delay during early zebrafish embryogenesis and a decrease in
544 fluorescence levels from a co-injected *DsRed* mRNA control reporter.
545 Interestingly, DjCas13d did not trigger a detectable 28S rRNA cleavage in these
546 conditions, suggesting that this uncontrolled effect may be more efficiently or
547 specifically generated by RfxCas13d. An additional alternative to CRISPR-Cas13
548 is type III CRISPR-Cas system based on Csm complexes that have been recently
549 employed to target RNA in human cells with minimal off-targets⁶¹. Although
550 similar approaches have been used in zebrafish embryos⁶², the multicomponent
551 factor of this CRISPR-Cas system with several proteins forming a functional
552 complex challenges its use as RNP particle or mRNA-gRNA formulation *in vivo*.
553 Another possibility to avoid collateral activity may be the application of
554 catalytically dead versions of Cas13 together with translational inhibitors to
555 silence mRNA expression instead of degrading them^{63,64}. Instead, we have
556 focused on the characterization, optimization and comparison of recently

557 described high-fidelity CRISPR-Cas systems to eliminate RNA but in an *in vivo*
558 context and using transient formulations that could be employed in potential RNA-
559 editing therapies^{65–72}. Further, it has been described that RfxCas13d induces an
560 immune response in humans⁷³ that could challenge the biomedical applications
561 of this technology. Whether DjCas13d or Cas7-11 trigger lower immunological
562 effects is something that remains to be determined. In summary, we demonstrate
563 that CRISPR-RfxCas13d is a robust, specific and efficient system to target RNAs
564 in zebrafish embryos but both CRISPR-Cas7-11 and CRISPR-DjCas13d RNP
565 complexes could also be employed specially when targeting exceptionally
566 abundant RNAs, being Cas7-11 less efficient than DjCas13d, although the latter
567 can still trigger developmental defects but in a lower degree than RfxCas13d.

568 Altogether, our optimizations will not only contribute to broaden and
569 enhance the use of RNA-targeting CRISPR-Cas approaches in zebrafish but also
570 will pave the way to optimize this technology *in vivo* for multiple biomedical and
571 biotechnological applications.

572

573 **Methods**

574 **Zebrafish maintenance.**

575 All experiments performed with zebrafish conform to national and
576 European Community standards for the use of animals in experimentation and
577 were approved by the Ethical committees from the Pablo de Olavide University,
578 CSIC and the Andalucian Government. Zebrafish wild type strains AB/Tübingen
579 (AB/Tu) or *Tupfel long fin* (TLF) were maintained and bred under standard
580 conditions⁷⁴. Natural mating of wild-type AB/Tu/TLF zebrafish adults (from 6 to
581 18 months) was used to collect the embryos for subsequent experiments.

582 Selection of mating pairs was random from a pool of 10 males and 10 females.
583 Zebrafish embryos were staged in hours post-fertilization (hpf) as described by
584 Kimmel *et al.* (1995)⁷⁵.

585

586 **Guide RNA design and mRNA generation.**

587 To design guide RNAs (gRNAs) used in this study (**Extended Data Table**
588 **1**), target mRNA sequences were analyzed *in silico* using RNAfold software⁷⁶
589 (<http://rna.tbi.univie.ac.at/cgi-bin/RNAWebSuite/RNAfold.cgi>) to select
590 protospacers of 23 (or 30) nucleotides with high accessibility (low base-pairing
591 probability from minimum free energy predictions) to generate gRNAs. All
592 designed gRNAs were synthesized by Synthego (Synthego Corp., CA, USA).
593 Three gRNAs targeting the same mRNA were co-injected, otherwise it is
594 specified in figure legends. *In vitro* transcribed (IVTed) RfxCas13d gRNAs were
595 generated like previously described^{7,8} but the amount of primers were reduced
596 by ten-fold in the fill in PCR (5 µL of 10 µM universal oligo and 5 µL of 10 µM of
597 specific oligos for a 50 µL fill-in PCR).

598

599 Heitag (RfxCas13d-hei) version⁴⁵ of RfxCas13d was generated by PCR
600 with Q5 High-Fidelity DNA polymerase (M0491, New England Biolabs) and
601 primers hei-tag_13d_Ncol_fwd and hei-tag_13d_SacII_rev containing a cmyc
602 tag, an oNLS and Ncol site in forward primer and an oNLS and SacII site in
603 reverse primer, and cloned into pT3TS-MCS (Addgene plasmid #31830)
604 backbone after digestion with restriction enzymes Ncol and SacII and ligation with
605 T4 DNA ligase (M0202, New England Biolabs). Similarly, bpNLS (mRfxCas13d-
606 bpNLS; Liang et al., 2022²⁷), optimized 2C-NLS (mRfxCas13d-2C-NLS; Liu et al.,

607 2019⁴²) and cmyc-2C-NLS (cmyc-mRfxCas13d-2C-NLS; Wu et al., 2019⁴³)
608 versions of *RfxCas13d* mRNA were created by PCR using primers
609 Ncol_13d_bpNLS_fwd / 13d_bpNLS_SacII_rev, Ncol_13d_fwd / 13d_2C-
610 NLS_SacII_rev and Ncol_13d_cmcy_fwd / 13d_2C-NLS_SacII_rev to add
611 bipartite NLS signals in N- and C-terminal ends, SV40 and nucleoplasmin long
612 (NLP) NLS signals in C-terminal end, and cmyc tag in N-terminal end and SV40
613 and NLP NLS signals in C-terminal end, respectively. Each fragment was then
614 cloned into pT3TS-NLS-RfxCas13d (Addgene plasmid #141321) backbone after
615 digestion with restriction enzymes Ncol and SacII. All primers are listed in
616 **Extended Data Table 2**. High-fidelity version of RfxCas13d (Hf-RfxCas13d) was
617 generated by site-directed mutagenesis using QuikChange Multi Site-Directed
618 Mutagenesis kit (Agilent), following manufacturer's instructions, and replicating
619 the amino acid changes described in Tong et al. (2023²⁵; N2V8 version). Primers
620 are listed in **Extended Data Table 2**.

621

622 To generate *RfxCas13d*, *RfxCas13d-NLS*, *RfxCas13d-hei*, *RfxCas13d-*
623 *bpNLS*, *RfxCas13d-2C-NLS*, *cmyc-RfxCas13d-2C-NLS* and *Hf-RfxCas13d*
624 mRNAs, the DNA templates were linearized using XbaI and mRNA was
625 synthesized using the mMachine T3 kit (Ambion) for 2 h. *In vitro* transcribed
626 mRNAs were then DNase-treated for 20 min with TURBO-DNAse at 37 °C,
627 purified using the RNeasy Mini Kit (Qiagen) and quantified using Nanodrop™
628 2000 (Thermo Fisher Scientific).

629

630

631

632 **Protein purification.**

633 The expression vector pET28b was used to clone genes for Hf-
634 RfxCas13d, DjCas13d and Cas7-11 proteins and were transformed into *E. coli*
635 Rosetta DE3 pRare competent cells (70954, EMD Millipore). DjCas13d ORF was
636 codon optimized for zebrafish using iCodon⁷⁷ (www.iCodon.org), purchased from
637 IDT (<https://eu.idtdna.com/>) and cloned into pET28b vector after Ncol / NotI
638 restriction enzyme digestion. Cas7-11 ORF was PCR amplified from pDF0229-
639 DiCas7-11 (Addgene plasmid #172506) with Q5 High-Fidelity DNA polymerase
640 (M0491, New England Biolabs; primers listed in **Extended Data Table 2**) and
641 cloned into pET28b. A freshly transformed colony was picked and grown over
642 night at 37 °C in LB supplemented with kanamycin and chloramphenicol. This
643 culture was diluted 100 times and grown at 37 °C until an OD₆₀₀ = 0.5 was
644 reached. At this point, cultures for Hf-RfxCas13d and DjCas13d expression were
645 induced with IPTG at a final concentration of 0.1 mM and incubated 3 h at 37 °C.
646 Culture for Cas7-11 expression was cooled for 30 minutes at 4 °C, induced with
647 IPTG at 0.3 mM and cultured over night at 18 °C. Protein purification was
648 performed as described in Hernández-Huertas *et al.* (2022⁸).

649

650 **Zebrafish embryo microinjection and image acquisition.**

651 One-cell stage zebrafish embryos were injected with 1-2 nL containing
652 300-600 pg of Cas13(s) mRNA or 3 ng of purified Cas protein and 300-1000 pg
653 of gRNA (see figure legends for details in each experiment). From 10 to 100 pg
654 of ectopic *gfp* mRNA and 75 pg of ectopic *dsRed* mRNA were injected for
655 collateral activity determination. Cas proteins and gRNAs were injected in two
656 rounds to maximize the amount of protein and gRNA (at the indicated

657 concentrations) per injection. Sequences of used gRNAs are indicated in

658 **Extended Data Table 1.**

659

660 For the miR-430 rescue experiment, mature miR-430 duplexes (**Extended**

661 **Data Table 2**) were purchased from IDT (<https://eu.idtdna.com/>) and

662 resuspended in RNase-free water. Embryos were injected with 1 nL of 2.5 or 5

663 µM miR-430 duplex solution (equimolar mix of 3 duplexes miR-430a, miR-430b

664 and miR-430c), using single-use aliquots.

665

666 Zebrafish embryo phenotypes and fluorescent pictures were analysed

667 using an Olympus SZX16 stereoscope and photographed with a Nikon DS-F13

668 digital camera. Images were processed with NIS-Elements D 4.60.00 software.

669 Phenotypes were quantified at 6, 24 or 48 hours post fertilization. GFP and

670 DsRed fluorescence were quantified using Fiji (Image J) software, using 15

671 embryos separated in three different images (5 embryos per quantified image).

672 Images were converted to 16-bit, background fluorescence was subtracted and

673 fluorescence levels were referred to the ones from embryos injected only with

674 reporter mRNAs.

675

676 **Protein sample preparation and Western Blot.**

677 Twenty embryos were collected at 6 hours post injection and washed twice

678 with deyolking buffer (55 mM NaCl, 1.8 mM KCl, and 1.25 mM NaHCO₃). Then,

679 samples were incubated for 5 min with orbital shaking and centrifuged at 300 g

680 for 30 s. Supernatant was removed and embryos were washed with buffer (110

681 mM NaCl, 3.5 mM KCl, 10 mM Tris-HCl pH 7.4, and 2.7 mM CaCl₂). Finally,

682 embryos were centrifuged again, and the supernatant was removed. The pellet
683 was resuspended in SDS-PAGE sample buffer (160 mM Tris-HCl pH 8, 20%
684 Glycerol, 2% SDS, 0.1% bromophenol blue, 200 mM DTT).

685

686 Sample separation by SDS-PAGE electrophoresis was performed using
687 10% TGX Stain-Free™ Fast Cast™ Acrylamide Solutions (Bio-Rad). After
688 electrophoresis, protein gel was activated in a Chemidoc MP (Bio-Rad) and
689 blotted onto a nitrocellulose membrane using the Trans-Blot Turbo Transfer
690 System (Bio Rad). The membrane was blocked for 1 h at room temperature in
691 Blocking Solution (5% fat free milk in 50 mM Tris-Cl, pH 7.5, 150 mM NaCl (TBS)
692 with 1% Tween20). Primary antibody Anti-HA (11867423001, Roche) and
693 secondary antibody anti-mouse HRP-labelled (A5278, Sigma-Aldrich) were
694 diluted 1:1000 and 1:5000 respectively in Blocking Solution. The membrane was
695 incubated in primary antibody solution overnight at 4 °C. After primary antibody
696 incubation, the membrane was washed three times in TBS with 1% Tween 20
697 (TTBS) for 10 min and incubated with the secondary antibody for 60 min at room
698 temperature. Washes were performed as with primary antibody. The protein
699 detection was done with Clarity™ Western ECL Substrate (Bio-Rad) and images
700 were acquired using a ChemiDoc MP (Bio-Rad).

701

702 qRT-PCR.

703 Ten zebrafish embryos per biological replicate were collected and snap
704 frozen in liquid nitrogen to analyze the expression level of the targeted mRNAs
705 by qRT-PCRs at the described hours post injection in figures or legends. Total
706 RNA was isolated using PRImeZOL™ Reagent protocol as described in the

707 manufacturer's instructions (Canvax Biotech). The cDNA was synthesized from
708 1000 ng of total RNA using iScript cDNA synthesis kit (Bio-Rad), following the
709 manufacturer's protocol. cDNA was 1/5 diluted and 2 µl was used per sample in
710 a 10 µl reaction containing 1.5 µl of forward and reverse primers (2 mM each;
711 **Extended Data Table 2**), 5 µl of SYBR® Premix Ex Taq (Tli RNase H Plus)
712 (Takara) and run in a CFX connect instrument (Bio-Rad). PCR cycling profile
713 consisted in a denaturing step at 95 °C for 30 s and 40 cycles at 95 °C for 10 s
714 and 60 °C for 30 s. *taf15* or *ef1α* mRNAs stably expressed along early
715 development were used as controls. To quantify *si:dkey-93m18.4* mRNA levels,
716 15 embryos per replicate were collected and snap-frozen in tubes containing 350
717 µL of TRIzol. Total RNA isolation was performed with the Zymo Direct-zol
718 Microprep kit according to manufacturers recommendations (including the DNase
719 digestion step), eluting in 20 µL of nuclease free H2O. Superscript IV was used
720 for reverse transcription of ~1 µg of total RNA, and resulting cDNA was diluted
721 1:20 for RT-qPCR. RT-qPCR was run in technical triplicate on a 384-well plate
722 setup by a Tecan robot and run on a QuantStudio 7 workstation using PerfeCTa®
723 SYBR® Green FastMix® (Quantabio). *cdk2ap2* mRNA stably expressed along
724 early development was used as control. Gene specific oligos for *si:dkey-93m18.4*
725 and *cdk2ap2* are listed in **Extended Data Table 2**.

726

727 To analyze the relative levels of *u4atac* snRNA, 15 embryos per replicate
728 were snap frozen and RNA samples enriched in small RNAs were obtained with
729 *mirVana* mRNA Isolation Kit (AM1561, ThermoFisher Scientific) following the
730 manufacturer's protocol. cDNA was synthesized from 100 ng of RNA using iScript
731 Select cDNA synthesis kit (Bio-Rad), following the manufacturer's protocol and

732 using the following miRNA universal primer (5'-
733 GCAGGTCCAGTTTTTTTTCTACCCC-3'), 2 µl of cDNA were used per
734 sample in a 10 µl reaction containing 1.5 µl of forward and reverse primers (2 mM
735 each; **Extended Data Table 2**), 5 µl of SYBR® Premix Ex Taq (Tli RNase H Plus)
736 (Takara) and run in a CFX connect instrument (Bio-Rad). PCR cycling profile
737 consisted in a denaturing step at 95 °C for 30 s and 40 cycles at 95 °C for 10 s
738 and 60 °C for 30 s. miR-430b mRNA was used as control.

739

740 ***In vivo RNA integrity analysis.***

741 RNA samples containing 10 embryos and purified using standard TRIzol
742 protocol, were submitted to RNA integrity analysis using Bioanalyzer Agilent 2100
743 (**Extended Data Fig. 3B, Extended Data Fig. 7A, B and G, Extended Data Fig.**
744 **7C and G, and Extended Data Fig. 9K-L**).

745

746 For *in vivo* RNA integrity analysis of IVTed gRNAs (**Fig. 2C-E and H and**
747 **Extended Data Fig. 8D**), 300-500 ng of total RNA was heat denatured for 2 min
748 at 70°C, placed on ice, and then loaded onto an RNA Nano Chip for the Agilent
749 Bioanalyzer 2100, prepared according to manufacturer's protocol.
750 Electrophoresis results were exported as image representations and as raw .csv
751 files of fluorescence intensity and time, including the ladder. Using R-Studio, the
752 ladder was fit with a second-degree polynomial and the polynomial fit was used
753 to calculate the size of the species in each experimental lane, resulting in a table
754 with traces of all RNA species represented by size in nucleotides and
755 fluorescence intensity. Size values fit with regions of the second-degree
756 polynomial with a negative derivative (including those of the 25 nt lower marker)

757 were then trimmed from these traces. A custom pipeline based around findpeaks
758 (pracma library) to detect, identify, quantify, and analyze up to the 3 most
759 prominent RNA species (18S, 28S, long 28S cleavage product) in each trace
760 (based on max-normalization) was developed and employed. If a species was
761 absent based on our peak calling results, the intensity within the search window
762 for that species was averaged and this mean intensity was used in calculating
763 the “28S rRNA integrity ratio”. In order to obtain reliable results of 28S rRNA
764 integrity ratio, all the samples must be run in the same gel electrophoresis within
765 the 2100 Bioanalyzer.

766

767 ***In vitro* RNA integrity analysis.**

768 A single *in vitro* experimental rRNA integrity assay (**Extended Data Fig.**
769 **3C-D**) consists of the following components in a 10 μ L reaction: 60 ng of
770 RfxCas13d protein, 500 ng of gRNA of interest, 300-500 ng zebrafish total RNA,
771 1 μ L of 10X CutSmart Buffer (New England Biolabs), and nuclease free water to
772 10 μ L. Reactions were incubated at 28.5°C for 45 minutes, heat denatured for 2
773 min at 70°C, placed on ice, and then 1 μ L of the reaction was loaded onto an
774 RNA Nano Chip for the Agilent Bioanalyzer 2100, prepared according to
775 manufacturer’s protocol. Electrophoresis results were exported as image
776 representations and as raw .csv files of fluorescence intensity and time, including
777 the ladder.

778

779 Using R-Studio, the ladder was fit with a second-degree polynomial and
780 trimmed traces as above. These traces were further timed to remove the gRNA
781 peak. *In vivo* rRNA analysis pipeline (see above) was modified and based around

782 findpeaks() (pracma library) to detect, identify, quantify, and analyze up to the 3
783 most prominent RNA species (18S, 28S, long 28S cleavage product) in each *in*
784 *vitro* trace (based on max-normalization). Due to the 10x lower input of RNA in
785 the *in vitro* traces, short 28S cleavage product was not detected above the
786 baseline. If a species was absent based on our peak calling results, the intensity
787 within the search window for that species were averaged and this mean intensity
788 was used in calculating the “28S rRNA integrity ratio”. In order to obtain reliable
789 results of 28S rRNA integrity ratio, all the samples must be run in the same gel
790 electrophoresis within the 2100 Bioanalyzer.

791

792 **RNA-seq libraries and analysis.**

793 Between 10 to 20 zebrafish embryos per biological replicate were collected
794 at 4 or 6 hpf and snap-frozen. For analyzing pri-miR430 targets stability with
795 optimized NLS version of RfxCas13d (**Fig. 3**) and to determine the collateral
796 activity induced by different CRISPR-Cas RNA targeting systems (**Figs. 5 and 6**,
797 **Extended Data Fig. 11**), total RNA was isolated using standard TRIzol protocol
798 as described in the manufacturer’s instructions (ThermoFisher Scientific) and
799 quantified using the Qubit fluorometric quantification (#Q10210, ThermoFisher
800 Scientific).

801

802 For pri-miR430 targets stability, 200 ng (except for 13.5 ng and 174 ng, for
803 two samples) of high-quality total RNA was used, as assessed using the
804 Bioanalyzer (Agilent), with the NEBNext Poly(A) mRNA Magnetic Isolation
805 Module (NEB, Cat. No. E7490L) at a 1/3rd reaction volume. Purified mRNA was
806 processed using the NEBNext Ultra II Directional RNA Library Prep Kit for

807 Illumina (NEB, Cat. No. E7760L) at a 1/10th reaction volume. Poly(A) isolated
808 mRNA was resuspended in 2.25 µL fragmentation mix and fragmented for 15 min
809 at 94°C then placed on ice for 2 min. First strand cDNA synthesis was performed
810 by manually transferring 1 µL of the fragmented mRNA into a 384 well Armadillo
811 PCR microplate (ThermoFisher, AB2396), containing 1 µL of the First Strand
812 cDNA synthesis reaction master mix aliquoted by the Mosquito HV Genomics
813 (SPT Labtech) nanoliter liquid-handling instrument. Second strand synthesis was
814 completed per protocol at the miniaturization scale and the cDNA was purified
815 using the SPRIselect bead-based reagent (Beckman Coulter, Cat. No. B23318)
816 at 1.8X with the Mosquito HV and eluted in 5 µL of 0.1X TE. Libraries were
817 generated using the NEBNext Ultra II Directional RNA Library Prep Kit at a 1/10th
818 reaction volume starting with 5 µL of cDNA. Adaptors were ligated by adding 500
819 nL of NEBNext Universal Adaptor diluted at 20-fold in supplied adaptor dilution
820 buffer. The adaptor-ligated material was PCR amplified with 14 cycles using the
821 NEBNext Multiplex Oligos for Illumina (96 Unique Dual Index Primer Pairs) (NEB,
822 Cat. No. E6442S) and the indexed libraries were purified using SPRIselect at
823 0.9X with the Mosquito HV and eluted in 10 µL of 0.1X TE.

824

825 For collateral activity RNAseq, mRNASeq libraries were generated from
826 100 ng (or ≤100 ng; RfxCas13d and DjCas13d) or 200 ng (or 40 ng for one
827 sample; Cas7-11) of high-quality total RNA, and analyzed using the Bioanalyzer
828 (Agilent). Libraries were made according to the manufacturer's directions using a
829 25-fold (or 100-fold) dilution of the universal adaptor and 12-16 cycles of PCR per
830 the respective masses with the NEBNext Ultra II Directional RNA Library Prep Kit
831 for Illumina (NEB, Cat. No. E7760L), the NEBNext Poly(A) mRNA Magnetic

832 Isolation Module (NEB, Cat. No. E7490L), and the NEBNext Multiplex Oligos for
833 Illumina (96 Unique Dual Index Primer Pairs) (NEB, Cat. No. E6440S) and
834 purified using the SPRiselect bead-based reagent (Beckman Coulter, Cat. No.
835 B23318).

836

837 Generated short fragment libraries for **Fig. 3, 5 and 6 and Extended Data**
838 **Fig. 11** were checked for quality and quantity using the Bioanalyzer and the Qubit
839 Flex Fluorometer (Life Technologies). Equal molar libraries were pooled,
840 quantified, and converted to process on the Singular Genomics G4 with the SG
841 Library Compatibility Kit, following the “Adapting Libraries for the G4 – Retaining
842 Original Indices” protocol. The converted pool was sequenced on an F3 flow cell
843 (Cat. No. 700125) on the G4 instrument with the PP1 and PP2 custom index
844 primers included in the SG Library Compatibility Kit (Cat. No. 700141), using
845 Instrument Control Software 23.08.1-1 with the following read length: 8 bp Index1,
846 100 bp Read1, and 8 bp Index2. Following sequencing, sgdemux 1.2.0 was run
847 to demultiplex reads for all libraries and generate FASTQ files.

848

849 To determine the number of gRNAs that can be injected together to detect
850 highly efficient gRNAs with CRISPR-RfxCas13d (**Extended Data Fig. 5**) and then
851 to analyze the prediction of *ex vivo* computational models using *in vivo* data from
852 200 gRNAs injected in sets of 25 gRNAs (**Fig. 4 and Extended Data Fig. 6**), total
853 RNA was isolated at 4 hpf using Direct-zol RNA Miniprep Kit (#R2050, Zymo
854 Research) following manufacturer’s instructions and quantified using the Qubit
855 fluorometric quantification (#Q10210, ThermoFisher Scientific). cDNA was
856 generated from 1.25 ng (2.5 ng for two replicates of RfxCas13d control samples)

857 of high-quality total RNA, as assessed using the Bioanalyzer (Agilent), according
858 to manufacturer's directions for the SMART-seq v4 Ultra Low Input RNA Kit
859 (Takara, 634891) at a 1/8th reaction volume (1/4th reaction volume for two
860 replicates of RfxCas13d control) and using the Mantis (Formulatrix) nanoliter
861 liquid-handling instrument to pipette the reagents for cDNA synthesis. Libraries
862 were generated manually (or with the Mosquito HV Genomics (SPT Labtech)
863 nanoliter liquid-handling instrument for RNAseq in **Fig. 4 and Extended Data**
864 **Fig. 6**), using the Nextera XT DNA Library Preparation Kit (Illumina, FC-131-
865 1096) at 1/8th reaction volumes paired with IDT for Illumina DNA/RNA UD
866 Indexes Set A (Illumina, 20027213), and purified using the Ampure XP bead-
867 based reagent (Beckman Coulter, Cat. No. A63882). Resulting short fragment
868 libraries were checked for quality and quantity using the Bioanalyzer and Qubit
869 Fluorometer (ThermoFisher). Equal molar libraries were pooled, quantified, and
870 sequenced on a High-Output flow cell of an Illumina NextSeq 500 instrument
871 using NextSeq Control Software 2.2.0.4 (or NextSeq Control Software 4.0.1 for
872 RNAseq in **Fig. 4 and Extended Data Fig. 6**) with the following read length: 70
873 bp Read1, 10 bp i7 Index and 10 bp i5 Index. Following sequencing, Illumina
874 Primary Analysis version NextSeq RTA 2.4.11 (or version NextSeq RTA 2.11.3.0
875 for RNAseq in **Fig. 4 and Extended Data Fig. 6**) and Secondary Analysis version
876 bcl2fastq2 v2.20 were run to demultiplex reads for all libraries and generate
877 FASTQ files.

878

879 RNA-seq reads were demultiplexed into Fastq format allowing up to one
880 mismatch using Illumina bcl-convert 3.10.5. Reads were aligned using STAR
881 version 2.7.3a to *Danio rerio* reference genome *danRer11* from University of

882 California at Santa Cruz (UCSC) with GFP exogenous sequence incorporated in
883 its index using Ensembl 106 gene models.

884

885 TPM (Transcript per Million) values were generated using RSEM version
886 1.3.0. Fold change for each gene was calculated using deseq2 (1.42.0) R
887 package after filtering genes with a count of less than 10 reads in all control
888 libraries. The resulting *p*-values were adjusted with Benjamini-Hochberg method
889 using R function p.adjust. For collateral activity assay, genes with less than 20
890 counts in the control conditions were filtered.

891

892 **Guide RNAs efficacy estimation.**

893 To determine the number of gRNAs that could be injected together in
894 zebrafish embryos to detect highly active gRNAs, we co-injected 10 and 25
895 gRNAs together with RfxCas13d protein in one-cell stage zebrafish embryos
896 (**Extended Data Table 1**). Then, RNAseq at 4 hpf were performed as described
897 earlier and gRNAs were divided into quintiles according to their activity (q5 and
898 q1 being the most and the least efficient gRNAs, respectively, **Extended Data**
899 **Fig. 5**).

900

901 To calculate gRNAs efficacy *in vivo*, 200 gRNAs (**Extended Data Table**
902 **1**) were injected in 8 different sets of 25 gRNAs together with RfxCas13d protein
903 in one-cell stage zebrafish embryos. Two to three gRNAs targeting the same
904 mRNA (75 mRNAs in total) were designed as described above, specifically to the
905 longest transcript isoform. gRNAs from set 1, set 2 and set 3 targeted the same
906 25 mRNAs, gRNAs from set 4, set 5 and set 6 targeted the following 25 mRNAs,

907 and gRNAs from set 7 and set 8 targeted the last 25 mRNAs. For instance, *aebp2*
908 transcript, one of the first 25 mRNAs, was targeted with gRNA1 (13d_aebp2_1)
909 in set 1, gRNA2 (13d_aebp2_1) in set 2 and gRNA3 (13d_aebp2_1) in set 3.
910 Then, *in vivo* gRNA efficacy for each individual gRNA was calculated as the
911 inverse of the Fold Change, obtained from RNAseq from zebrafish embryos at 4
912 hpf.

913

914 The most recent and updated computational models to predict CRISPR-
915 RfxCas13d activity generated from *ex vivo* cell culture data, TIGER¹⁷,
916 DeepCas13¹⁸ and RNAtargeting¹⁹, were used to estimate gRNA efficacy. Since
917 RNAtargeting generates gRNA spacer sequences of 30 nt length, the first 23 nt
918 from the 5' end were used to make them comparable to our gRNAs and to other
919 models. Out of 200 gRNA used in this experiment, including 3 gRNAs as negative
920 controls, 191 were compatible to be analyzed in all computational models. Then,
921 the performance of each prediction model was evaluated using Pearson's
922 correlation coefficient. *Ex vivo* cell culture data from 396 gRNAs targeting *gfp*
923 mRNA¹⁶ was used as an external control.

924

925 **Statistical analyses.**

926 All statistical analyses were performed without predetermining sample
927 size. The experiments were not randomized, and investigators were not blinded
928 to allocation during experiments and outcome assessment. No data was
929 excluded from the analysis. Number of embryos, replicates and experiments are
930 indicated in figures and/or figure legends.

931

932 For phenotypes derived from embryo microinjections, Xi-square or Fisher
933 statistical analyses were undertaken using GraphPad Prism 8 (La Jolla, CA,
934 USA). For qRT-PCR and GFP and DsRed fluorescence levels, T-test statistical
935 analyses were performed. *p*-values are indicated in figures or figure legends.
936 Non-parametric Mann-Whitney U statistical tests were performed to compare
937 high (top 5) and low (bottom 5) active gRNAs scores (**Fig. 4C-E**).

938

939 *p*-values and distances (D, maximal vertical distance between the compared
940 distribution) for the comparison of the cumulative distribution of RNA levels at 6
941 hpf (**Fig. 3C**) were calculated using Kolmogorov-Smirnov Tests by dgof (v 1.4) in
942 R package.

943

944 **Data availability**

945 Sequencing data have been uploaded to Gene Expression Omnibus
946 (GEO) (Series GSE270724). Imaging and raw data are available upon request.
947 All other data is available in the main text or the supplementary information.

948

949 **Acknowledgements**

950 We thank all members of the Moreno-Mateos laboratory for intellectual and
951 technical support. This work was supported by Ramon y Cajal (RyC-2017-
952 23041), PID2021-127535NB-I00, CNS2022-135564 and CEX2020-001088-M
953 grants funded by MICIU/AEI/ 10.13039/501100011033 by “ERDF A way of
954 making Europe” (“ERDF/EU”), and by ESF Investing in your future from Ministerio
955 de Ciencia, Innovación y Universidades and European Union (M.A.M.-M.). This
956 work has also been co-financed by the Spanish Ministry of Science and

957 Innovation with funds from the European Union NextGenerationEU (PRTR-
958 C17.I1) and the Regional Ministry of University, Research and Innovation of the
959 Autonomous Community of Andalusia within the framework of the Biotechnology
960 Plan applied to Health. The Moreno-Mateos lab was also funded by European
961 Regional Development Fund (FEDER 80% of the total funding) by the Ministry of
962 Economy, Knowledge, Business and University, of the Government of Andalusia,
963 within the framework of the FEDER Andalusia 2014-2020 operational program
964 within the objective "Promotion and generation of frontier knowledge and
965 knowledge oriented to the challenges of society, development of emerging
966 technologies (grant UPO-1380590)". M.A.M.-M. was the recipient of the Genome
967 Engineer Innovation 2019 Grant from Synthego. The CABD is an institution
968 funded by University Pablo de Olavide, Consejo Superior de Investigaciones
969 Científicas (CSIC), and Junta de Andalucía. I.M-S. was a recipient of the
970 Margarita Salas Postdoctoral contract funded by "NextGenerationEU", Plan de
971 Recuperación, Transformación y Resilencia and Ministerio de Ciencia,
972 Innovación y Universidades (recualificación del sistema universitario español
973 2021-2023, Pablo de Olavide University Call). L.H-H. and D.N-C. were recipients
974 of Ayudas para contratos predoctorales para la formación de doctores (Ministerio
975 de Ciencia e Innovación) funded by MICIU/AEI /10.13039/501100011033 and
976 FSE invierte en tu futuro and FSE. C.G-M. was funded with Ayudas captación,
977 incorporación y movilidad de capital humano de I+D+i, Junta de Andalucía
978 (POSTDOC 21_00667). P.M.M.G. was funded by a postdoctoral fellowship from
979 Junta de Andalucía (DOC_00397). This study was supported by the Stowers
980 Institute for Medical Research. A.A.B. was awarded a US National Institutes of
981 Health grant (NIH-R01 GM136849 and NIH R21OD034161). A.J.T. was

982 supported by the US National Institute of Health: F31HD110268. This work was
983 completed as part of thesis research for A.J.T. & G.dS.P., Graduate School of the
984 Stowers Institute for Medical Research. This work was supported by grant
985 PID2021-125682NB-I00 to M.A.N. funded by MICIU/AEI
986 /10.13039/501100011033 and by FEDER, UE, and by Instituto de Salud Carlos
987 III (CIBERER, CB19/07/00038 to MAN), who also acknowledges financial support
988 from the Spanish State Research Agency, through the "Severo Ochoa Program"
989 for Centres of Excellence in R&D Grant CEX2021-001165-S funded by
990 MCIN/AEI/ 10.13039/501100011033. M.J.M. was supported by grant PID2020-
991 120463RB-I00 funded by the Spanish Ministerio de Ciencia e Innovación. We
992 thank our colleague Francisco J. Guerra (Stowers Institute and CABD) for the
993 initial research on Cas7-11. We also thank Rhonda Egidy and Anoja Perera from
994 Sequencing and Discovery Genomics at Stowers (Kansas, MO, USA).
995

996 **Author contributions**

997 M.A.M-M. conceived the project and designed the research. I.M-S., L.H-
998 H. and D.N-C. performed most of the experiments. C.G-M., A.C-R. and M.J.M.
999 contributed in the CRISPR-Cas7-11 experiments and analysis. A.J.T., G.dS.P.
1000 and G.K. performed part of the experiments and analyzed the results from *in vitro*
1001 transcribed gRNAs assays. L.T-G. and A.D-M. performed protein purifications.
1002 J.A.W.II produced the synthetic gRNAs. K.H helped with cm-gRNAs section
1003 together with J.G. and M.A.N. that also contributed with the optimization of
1004 RfxCas13d-NLS. P.M.M-G. performed gRNA activity prediction analysis and
1005 computational models' comparison. M.A.M-M. I.M-S., L.H-H. and D.N-C. carried
1006 out data analysis with the help of A.A.B. M.A.M-M. and I.M-S. wrote the

1007 manuscript with the contribution of L.H-H., D.N-C. and A.A.B. and with the input
1008 from the other authors. All authors reviewed and approved the manuscript.

1009

1010 **Declaration of interests**

1011 Kevin Holden and John A. Walker II were both employees and
1012 shareholders in Synthego Corporation at the time of this work. The rest of authors
1013 declares no competing interests.

1014

1015

1016 **References**

1017

- 1018 1. Wessels, H. H. *et al.* Efficient combinatorial targeting of RNA transcripts in
1019 single cells with Cas13 RNA Perturb-seq. *Nat Methods* **20**, 86–94 (2023).
- 1020 2. Montero, J. J. *et al.* Genome-scale pan-cancer interrogation of lncRNA
1021 dependencies using CasRx. *Nat Methods* (2024) doi:10.1038/S41592-024-
1022 02190-0.
- 1023 3. Tieu, V. *et al.* A versatile CRISPR-Cas13d platform for multiplexed
1024 transcriptomic regulation and metabolic engineering in primary human T
1025 cells. *Cell* **187**, 1278-1295.e20 (2024).
- 1026 4. Ding, Y., Tous, C., Choi, J., Chen, J. & Wong, W. W. Orthogonal inducible
1027 control of Cas13 circuits enables programmable RNA regulation in
1028 mammalian cells. *Nat Commun* **15**, (2024).
- 1029 5. Zhou, H. *et al.* Glia-to-Neuron Conversion by CRISPR-CasRx Alleviates
1030 Symptoms of Neurological Disease in Mice. *Cell* **181**, 590-603.e16 (2020).
- 1031 6. Powell, J. E. *et al.* Targeted gene silencing in the nervous system with
1032 CRISPR-Cas13. *Sci Adv* **8**, 2485 (2022).
- 1033 7. Kushawah, G. *et al.* CRISPR-Cas13d Induces Efficient mRNA Knockdown
1034 in Animal Embryos. *Dev Cell* **54**, 805-817.e7 (2020).
- 1035 8. Hernandez-Huertas, L. *et al.* Optimized CRISPR-RfxCas13d system for
1036 RNA targeting in zebrafish embryos. *STAR Protoc* **3**, (2022).
- 1037 9. Zhu, W. *et al.* Reading and writing of mRNA m6A modification orchestrate
1038 maternal-to-zygotic transition in mice. *Genome Biol* **24**, (2023).
- 1039 10. Shangguan, H., Huang, X., Lin, J. & Chen, R. Knockdown of Kmt2d leads
1040 to growth impairment by activating the Akt/β-catenin signaling pathway. *G3*
1041 *Genes|Genomes|Genetics* (2024) doi:10.1093/G3JOURNAL/JKAD298.
- 1042 11. Cheng, R. *et al.* Modification of alternative splicing in bovine somatic cell
1043 nuclear transfer embryos using engineered CRISPR-Cas13d. *Science China Life Sciences* 2022 **65**:11 65, 2257–2268 (2022).

- 1045 12. Bi, D. *et al.* CRISPR/Cas13d-mediated efficient KDM5B mRNA knockdown
1046 in porcine somatic cells and parthenogenetic embryos. *Reproduction* **162**,
1047 149 (2021).
- 1048 13. Del Prado, J. A.-N. *et al.* Comparing robotic and manual injection methods
1049 in zebrafish embryos for high-throughput RNA silencing using CRISPR-
1050 RfxCas13d. *Biotechniques* **76**, (2024).
- 1051 14. Hernandez-Huertas, L. *et al.* CRISPR-RfxCas13d screening uncovers
1052 Bckdk as a post-translational regulator of the maternal-to-zygotic transition
1053 in teleosts. *bioRxiv* (2024) doi:10.1101/2024.05.22.595167.
- 1054 15. Nishimura, T., Takahashi, E. & Fujimoto, T. Sterilization of fish through
1055 adaptable gRNAs targeting dnd1 using CRISPR-Cas13d system.
1056 *Aquaculture* **593**, 741269 (2024).
- 1057 16. Wessels, H. H. *et al.* Massively parallel Cas13 screens reveal principles for
1058 guide RNA design. *Nat Biotechnol* **38**, 722–727 (2020).
- 1059 17. Wessels, H. H. *et al.* Prediction of on-target and off-target activity of
1060 CRISPR–Cas13d guide RNAs using deep learning. *Nat Biotechnol* (2023)
1061 doi:10.1038/s41587-023-01830-8.
- 1062 18. Cheng, X. *et al.* Modeling CRISPR-Cas13d on-target and off-target effects
1063 using machine learning approaches. *Nature Communications* **2023** *14*:1
1064 **14**, 1–14 (2023).
- 1065 19. Wei, J. *et al.* Deep learning and CRISPR-Cas13d ortholog discovery for
1066 optimized RNA targeting. *Cell Syst* **14**, 1087-1102.e13 (2023).
- 1067 20. Moreno-Mateos, M. A. *et al.* CRISPRscan: Designing highly efficient
1068 sgRNAs for CRISPR-Cas9 targeting in vivo. *Nat Methods* **12**, 982–988
1069 (2015).
- 1070 21. Doench, J. G. *et al.* Optimized sgRNA design to maximize activity and
1071 minimize off-target effects of CRISPR-Cas9. *Nat Biotechnol* **34**, 184–191
1072 (2016).
- 1073 22. Kim, H. K. *et al.* Deep learning improves prediction of CRISPR-Cpf1 guide
1074 RNA activity. *Nat Biotechnol* **36**, 239–241 (2018).
- 1075 23. Buchman, A. *et al.* Programmable RNA Targeting Using CasRx in Flies.
1076 *CRISPR J* **3**, 164 (2020).
- 1077 24. Huynh, N., Depner, N., Larson, R. & King-Jones, K. A versatile toolkit for
1078 CRISPR-Cas13-based RNA manipulation in Drosophila. *Genome Biol* **21**,
1079 (2020).
- 1080 25. Tong, H. *et al.* High-fidelity Cas13 variants for targeted RNA degradation
1081 with minimal collateral effects. *Nat Biotechnol* (2022) doi:10.1038/s41587-
1082 022-01419-7.
- 1083 26. Shi, P. *et al.* Collateral activity of the CRISPR/RfxCas13d system in human
1084 cells. *Commun Biol* **6**, 334 (2023).
- 1085 27. Ai, Y., Liang, D. & Wilusz, J. E. CRISPR/Cas13 effectors have differing
1086 extents of off-target effects that limit their utility in eukaryotic cells. *Nucleic
1087 Acids Res* **50**, E65–E65 (2022).
- 1088 28. Kelley, C. P., Haerle, M. C. & Wang, E. T. Negative autoregulation mitigates
1089 collateral RNase activity of repeat-targeting CRISPR-Cas13d in
1090 mammalian cells. *Cell Rep* **40**, (2022).
- 1091 29. Li, Y. *et al.* The collateral activity of RfxCas13d can induce lethality in a
1092 RfxCas13d knock-in mouse model. *Genome Biol* **24**, (2023).

- 1093 30. Meeske, A. J., Nakandakari-Higa, S. & Marraffini, L. A. Cas13-induced
1094 cellular dormancy prevents the rise of CRISPR-resistant bacteriophage.
1095 *Nature* **570**, 241–245 (2019).
- 1096 31. East-Seletsky, A. et al. Two distinct RNase activities of CRISPR-C2c2
1097 enable guide-RNA processing and RNA detection. *Nature* **538**, 270–273
1098 (2016).
- 1099 32. Abudayyeh, O. O. et al. C2c2 is a single-component programmable RNA-
1100 guided RNA-targeting CRISPR effector. *Science* (1979) **353**, (2016).
- 1101 33. Zhang, C. et al. Structural basis for the RNA-guided ribonuclease activity
1102 of CRISPR-Cas13d. *Cell* **175**, 212 (2018).
- 1103 34. Slaymaker, I. M. et al. High-resolution structure of Cas13b and biochemical
1104 characterization of RNA targeting and cleavage. *Cell Rep* **26**, 3741 (2019).
- 1105 35. Escot, S., Elouin, A., Mellottee, L. & David, N. B. Nhs1b regulates
1106 mesodermal cell migration by controlling protrusion dynamics during
1107 zebrafish gastrulation. *bioRxiv* 2023.01.28.526006 (2023)
1108 doi:10.1101/2023.01.28.526006.
- 1109 36. Méndez-Mancilla, A. et al. Chemically modified guide RNAs enhance
1110 CRISPR-Cas13 knockdown in human cells. *Cell Chem Biol* **0**, (2021).
- 1111 37. White, R. J. et al. A high-resolution mRNA expression time course of
1112 embryonic development in zebrafish. *Elife* **6**, e30860–e30860 (2017).
- 1113 38. Sun, Q., Hao, Q. & Prasantha, K. V. Nuclear long noncoding RNAs: key
1114 regulators of gene expression. *Trends Genet* **34**, 142 (2018).
- 1115 39. Guh, C. Y., Hsieh, Y. H. & Chu, H. P. Functions and properties of nuclear
1116 IncRNAs—from systematically mapping the interactomes of IncRNAs. *J
1117 Biomed Sci* **27**, 1–14 (2020).
- 1118 40. Pillay, S., Takahashi, H., Carninci, P. & Kanhere, A. Antisense RNAs during
1119 early vertebrate development are divided in groups with distinct features.
1120 *Genome Res* **31**, 995–1010 (2021).
- 1121 41. Konermann, S. et al. Transcriptome Engineering with RNA-Targeting Type
1122 VI-D CRISPR Effectors. *Cell* **173**, 665-676.e14 (2018).
- 1123 42. Liu, P. et al. Enhanced Cas12a editing in mammalian cells and zebrafish.
1124 *Nucleic Acids Res* **47**, 4169–4180 (2019).
- 1125 43. Wu, Y. et al. Highly efficient therapeutic gene editing of human
1126 hematopoietic stem cells. *Nat Med* **25**, 776 (2019).
- 1127 44. Liang, F. et al. SpG and SpRY variants expand the CRISPR toolbox for
1128 genome editing in zebrafish. *Nature Communications* 2022 13:1 **13**, 1–10
1129 (2022).
- 1130 45. Thumberger, T. et al. Boosting targeted genome editing using the hei-tag.
1131 *Elife* **11**, (2022).
- 1132 46. Giraldez, A. J. et al. Zebrafish MiR-430 Promotes Deadenylation and
1133 Clearance of Maternal mRNAs. Source: *Science, New Series* vol. 312
1134 (2006).
- 1135 47. Giraldez, A. J. et al. MicroRNAs regulate brain morphogenesis in zebrafish.
1136 *Science* **308**, 833–838 (2005).
- 1137 48. Hadzhiev, Y. et al. The miR-430 locus with extreme promoter density forms
1138 a transcription body during the minor wave of zygotic genome activation.
1139 *Dev Cell* **58**, 155–170.e8 (2023).
- 1140 49. Medina-Muñoz, S. G. et al. Crosstalk between codon optimality and cis-
1141 regulatory elements dictates mRNA stability. *Genome Biol* **22**, 1–23 (2021).

- 1142 50. Vejnar, C. E. *et al.* Genome wide analysis of 3' UTR sequence elements
1143 and proteins regulating mRNA stability during maternal-to-zygotic transition
1144 in zebrafish. *Genome Res* **29**, 1100–1114 (2019).
- 1145 51. Khatri, D. *et al.* Deficiency of the minor spliceosome component U4atac
1146 snRNA secondarily results in ciliary defects in human and zebrafish. *Proc
1147 Natl Acad Sci U S A* **120**, (2023).
- 1148 52. Özcan, A. *et al.* Programmable RNA targeting with the single-protein
1149 CRISPR effector Cas7-11. *Nature* **597**, 720–725 (2021).
- 1150 53. Rossi, A. *et al.* Genetic compensation induced by deleterious mutations but
1151 not gene knockdowns. *Nature* **524**, 230–233 (2015).
- 1152 54. Housden, B. E. *et al.* Loss-of-function genetic tools for animal models:
1153 cross-species and cross-platform differences. *Nature Reviews Genetics*
1154 **2016** *18*:1 24–40 (2016).
- 1155 55. Bosch, B. *et al.* Genome-wide gene expression tuning reveals diverse
1156 vulnerabilities of M. tuberculosis. *Cell* **184**, 4579-4592.e24 (2021).
- 1157 56. Saunders, L. M. *et al.* Embryo-scale reverse genetics at single-cell
1158 resolution. *Nature* **623**, 782 (2023).
- 1159 57. Huang, H., Liu, C., Wagle, M. M. & Yang, P. Evaluation of deep learning-
1160 based feature selection for single-cell RNA sequencing data analysis.
Genome Biol **24**, (2023).
- 1161 58. Shen, W. *et al.* Comprehensive maturity of nuclear pore complexes
1162 regulates zygotic genome activation. *Cell* **185**, 4954-4970.e20 (2022).
- 1163 59. Haeussler, M. *et al.* Evaluation of off-target and on-target scoring
1164 algorithms and integration into the guide RNA selection tool CRISPOR.
Genome Biol **17**, (2016).
- 1165 60. Hart, S. K. *et al.* Low copy CRISPR-Cas13d mitigates collateral RNA
1166 cleavage. *bioRxiv* (2024) doi:10.1101/2024.05.13.594039.
- 1167 61. Colognori, D., Trinidad, M. & Doudna, J. A. Precise transcript targeting by
1168 CRISPR-Csm complexes. *Nat Biotechnol* **41**, 1256 (2023).
- 1169 62. Fricke, T. *et al.* Targeted RNA Knockdown by a Type III CRISPR-Cas
1170 Complex in Zebrafish. *CRISPR J* **3**, 299 (2020).
- 1171 63. Li, S. *et al.* Screening for functional circular RNAs using the CRISPR-Cas13
1172 system. *Nat Methods* **18**, 51–59 (2021).
- 1173 64. Apostolopoulos, A. *et al.* dCas13-mediated translational repression for
1174 accurate gene silencing in mammalian cells. *Nat Commun* **15**, (2024).
- 1175 65. Zhu, Y., Zhu, L., Wang, X. & Jin, H. RNA-based therapeutics: an overview
1176 and prospectus. *Cell Death & Disease* **2022** *13*:7 **13**, 1–15 (2022).
- 1177 66. Balwani, M. *et al.* Phase 3 Trial of RNAi Therapeutic Givosiran for Acute
1178 Intermittent Porphyria. *New England Journal of Medicine* **382**, 2289–2301
1179 (2020).
- 1180 67. Schultheis, B. *et al.* First-in-human phase I study of the liposomal RNA
1181 interference therapeutic Atu027 in patients with advanced solid tumors.
Journal of Clinical Oncology **32**, 4141–4148 (2014).
- 1182 68. Kumar, S. *et al.* RNA-targeting strategies as a platform for ocular gene
1183 therapy. *Prog Retin Eye Res* **92**, (2023).
- 1184 69. Li, J. *et al.* Cas13b-mediated RNA targeted therapy alleviates genetic
1185 dilated cardiomyopathy in mice. *Cell Biosci* **14**, (2024).
- 1186 70. Keng, C. T. *et al.* AAV-CRISPR-Cas13 eliminates human enterovirus and
1187 prevents death of infected mice. *EBioMedicine* **93**, 104682 (2023).

- 1191 71. Li, J. *et al.* A high-fidelity RNA-targeting Cas13 restores paternal Ube3a
1192 expression and improves motor functions in Angelman syndrome mice.
1193 *Molecular Therapy* **31**, 2286–2295 (2023).
- 1194 72. Cui, Z. *et al.* Cas13d knockdown of lung protease Ctsl prevents and treats
1195 SARS-CoV-2 infection. *Nat Chem Biol* **18**, 1056–1064 (2022).
- 1196 73. Tang, X. Z. E., Tan, S. X., Hoon, S. & Yeo, G. W. Pre-existing adaptive
1197 immunity to the RNA-editing enzyme Cas13d in humans. *Nat Med* **28**, 1372
1198 (2022).
- 1199 74. Daude, N. *et al.* Knockout of the prion protein (PrP)-like Sprn gene does
1200 not produce embryonic lethality in combination with PrPC-deficiency. *Proc
1201 Natl Acad Sci U S A* **109**, 9035–9040 (2012).
- 1202 75. Kimmel, C. B., Ballard, W. W., Kimmel, S. R., Ullmann, B. & Schilling, T. F.
1203 Stages of embryonic development of the zebrafish. *Developmental
1204 Dynamics* **203**, 253–310 (1995).
- 1205 76. Lorenz, R. *et al.* ViennaRNA Package 2.0. *Algorithms Mol Biol* **6**, (2011).
- 1206 77. Diez, M. *et al.* iCodon customizes gene expression based on the codon
1207 composition. *Scientific Reports* 2022 **12**:1 1–16 (2022).
- 1208

Moreno-Sánchez, Hernández-Huertas, Nahón-Cano et al. Fig. 1

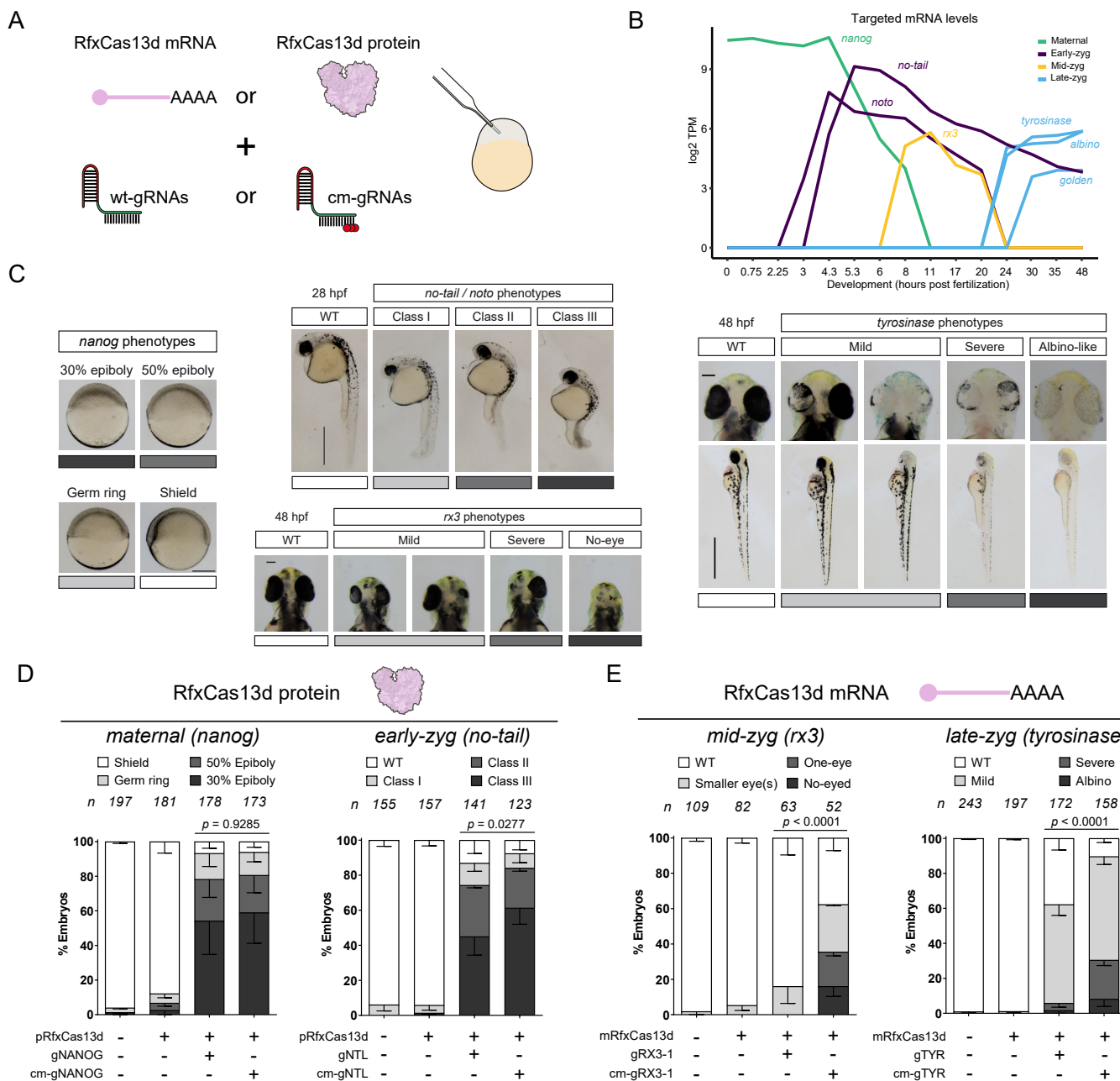


Figure 1. Sustained CRISPR-RfxCas13d targeting in zebrafish embryos.

- A)** Schematic illustration of the experimental setup used to compare CRISPR-RfxCas13d activity using standard (wt-gRNAs) or chemically modified (cm-gRNAs) gRNAs, with both mRNA (*RfxCas13d* mRNA) and purified protein (RfxCas13d protein). One-cell stage zebrafish embryos were injected with 300 pg of RfxCas13d mRNA or 3 ng of RfxCas13d protein together with 1 ng of a mix of three gRNAs (~300 pg from each gRNA) (otherwise indicated in the corresponding figure legend).
- B)** Expression levels (log₂ TPM: Transcript per million reads) during the first 48 hours post-fertilization (hpf) of the different maternally-provided (*nanog*) and zygotically-expressed (*tbxta – no-tail*, *noto*, *rx3*, *tyrosinase*, *slc45a2 – albino*, and *slc24a5 – golden*) mRNAs targeted in this study. Early-zyg, Mid-zyg and Late-zyg indicate early, mid and late zygotically-expressed mRNAs, respectively. Data from zebrafish Expression Atlas³⁷. TPM values lower than 10 were referred as 0.
- C)** Representative images of the phenotypes obtained after the injection of the mRNA-gRNAs or ribonucleoprotein (RNP) complexes targeting the indicated maternally-provided or zygotically-expressed mRNAs. *Nanog* loss-of-function phenotypes were evaluated at ~6 hpf: 30% epiboly, 50% epiboly, germ ring, and shield stages correspond to 4.6, 5.3, 5.7, and 6 hpf in non-injected embryos growing in standard conditions, respectively (scale bar, 0.25 mm). *Tbxta – no-tail* or *noto* loss-of-function phenotypes were evaluated at 28 hpf (scale bar, 0.5 mm). Class I: short tail (least extreme), Class II: absence of notochord and short tail (medium level), and Class III: absence of notochord and extremely short tail (most extreme). *Rx3*, loss-of-function phenotypes were evaluated at 48 hpf (scale bar, 0.1 mm). Mild: smaller eye(s) (least extreme), Severe: absence of one eye (medium level), and No-eye: absence of both eyes (most extreme). *Tyrosinase* loss-of-function phenotypes (reduced or lack of pigmentation) were evaluated at 48 hpf (scale bar, 0.75 mm for lateral views and 0.1 mm for insets). Mild (least extreme), Severe (medium level), and Albino-like (most extreme).
- D)** Stacked barplots showing percentage of observed phenotypes in zebrafish embryos injected with standard or cm-gRNAs targeting *nanog* (gNANOG) and *no-tail* (gNTL) together with RfxCas13d protein (pRfxCas13d). (n) total number of embryos is shown for each condition. The results are shown as the averages ± standard deviation of the mean of each phenotypic category from at least two

independent experiments. Chi-square (χ^2) statistical tests were performed to compare standard and cm-gRNAs.

E) Stacked barplots showing percentage of observed phenotypes in zebrafish embryos injected with standard or cm-gRNAs targeting *rx3* (one single gRNA, gRX3-1) and *tyrosinase* (gTYR) together with RfxCas13d mRNA (mRfxCas13d). (n) total number of embryos is shown for each condition. The results are shown as the averages \pm standard deviation of the mean of each phenotypic category from at least two independent experiments. χ^2 statistical tests were performed to compare standard and cm-gRNAs.

Moreno-Sánchez, Hernández-Huertas, Nahón-Cano et al. Fig. 2

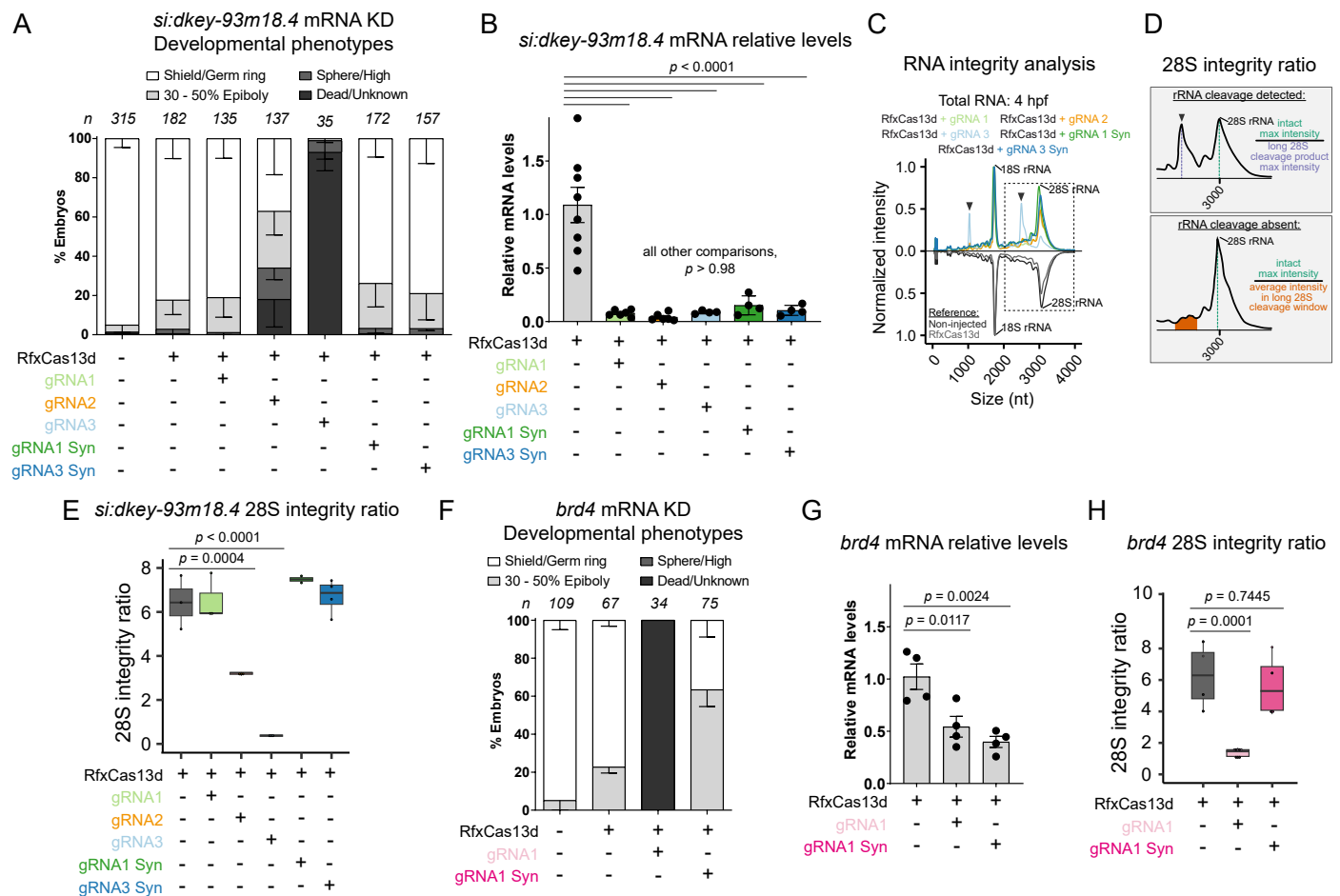


Figure 2. *In vitro* transcribed gRNAs can induce toxicity.

- A)** Stacked barplots showing percentage of developmental effect of *si:dkey-93m18.4* KD at 6 hpf using *in vitro* transcribed gRNAs (IVT_{ed}, gRNAs 1-3) or chemically synthetized (Syn) gRNAs (400 pg/embryo). (n) total number of embryos is shown for each condition. The results are shown as the averages ± standard deviation of the mean of each developmental stage from at least two independent experiments.
- B)** Boxplot showing relative *si:dkey-93m18.4* mRNA levels measured by qRT-PCR at 4 hpf from injected embryos in **A**. Results are shown as the averages ± standard deviation of the mean from at least four biological replicates from two independent experiments. One-way ANOVA followed by Tukey post-hoc analysis was performed. *cdk2ap2* mRNA was used as a normalization control.
- C)** Mirrored line-plot represents relative abundance (normalized fluorescence intensity of bioanalyzer electrophoresis) of RNA species present in total RNA at 4 hpf from RfxCas13d mediated *si:dkey-93m18.4* KD and control embryos. Traces are single replicates. Non-injected (gray) and RfxCas13d alone (black) traces are inverted as a reference for RfxCas13d + gRNA1 (light green), RfxCas13d + gRNA2 (orange), RfxCas13d + gRNA3 (light blue), RfxCas13d + gRNA1 Syn (dark green), and RfxCas13d + gRNA3 Syn (dark blue). Black arrows denote peaks from 28S rRNA cleavage.
- D)** Cartoon of 28S integrity ratio calculation as the intensity of the 28S rRNA relative to the long 28S cleavage product when was detected (top) and when it was absent (bottom). See Methods for further details.
- E)** Boxplot of 28S integrity ratio *in vivo* at 4 hpf from RfxCas13d mediated *si:dkey-93m18.4* KD and control embryos. At least two biological replicates were analyzed. The mean, first and third quartile are represented for each condition. One-way ANOVA followed by Dunnett's post-hoc analysis was performed.
- F)** Stacked barplots showing percentage of developmental effect of *brd4* KD at 6 hpf using an *in vitro* transcribed or chemically synthetized gRNA (IVT_{ed}, gRNA1 and Syn, respectively; 300 pg of gRNA/embryo). (n) total number of embryos is shown for each condition. The results are shown as the averages ± standard

deviation of the mean of each developmental stage from at least two independent experiments.

G) Boxplot showing relative *brd4* mRNA levels measured by qRT-PCR at 4 hpf from injected embryos in F. The mean, first and third quartile are represented for each condition. Four biological replicates from two independent experiments were analyzed. One-way ANOVA was performed. *taf15* mRNA was used as a normalization control.

H) Boxplot of 28S integrity ratio *in vivo* at 4 hpf from RfxCas13d mediated *brd4* KD and control embryos. The mean, first and third quartile are represented for each condition. At least four biological replicates were analyzed. One-way ANOVA followed by Dunnett's post-hoc analysis was performed.

Moreno-Sánchez, Hernández-Huertas, Nahón-Cano et al. Fig. 3

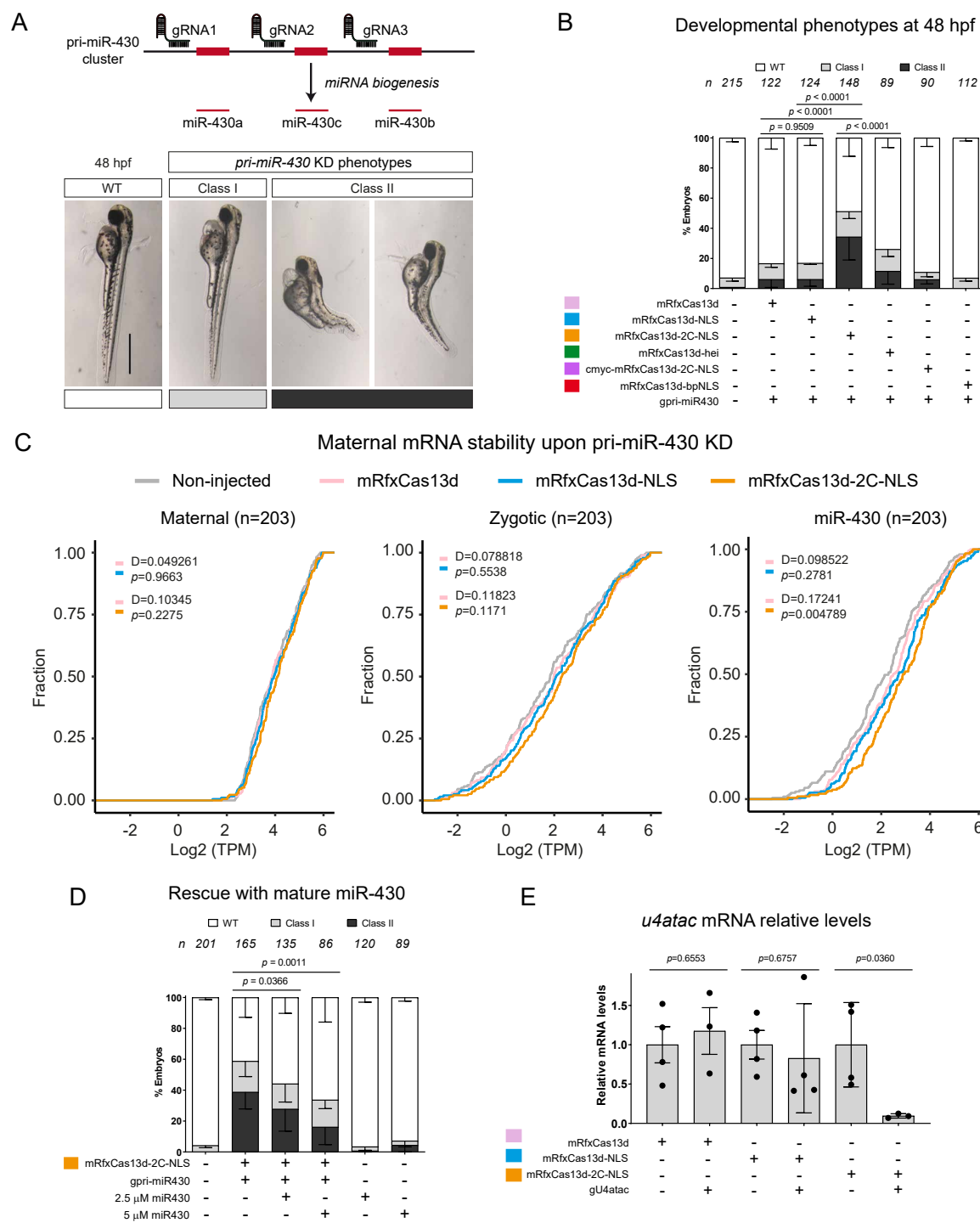


Figure 3. An optimized localization signal enhances CRISPR-RfxCas13d nuclear RNA-targeting.

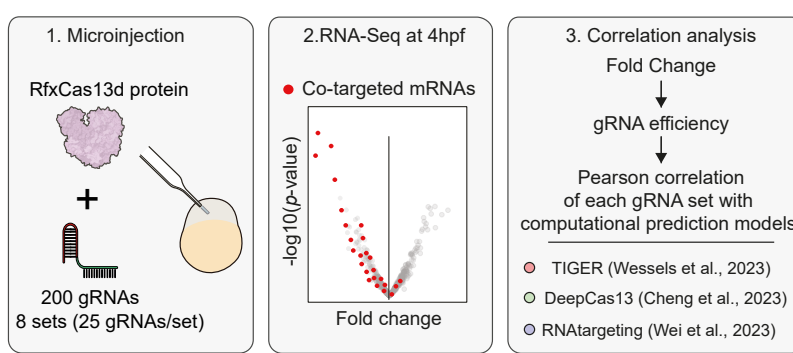
- A)** Diagram illustrating the positions of three gRNAs targeting primary miR430 transcript (pri-miR430), red rectangles indicate the mature microRNAs (miR430a, miR430b, and miR430c). Scheme based on Hadzhiev et al., 2023⁴⁸ (top). Representative images of developmental defects observed at 48 hpf when targeting miR430 (scale bar, 0.75 mm) (bottom). Class I: heart oedema (least extreme), and Class II: body curvature and/or tail blister (most extreme).
- B)** Stacked barplots showing percentage of observed phenotypes at 48 hpf comparing cytoplasmic (mRfxCas13d, pink), NLS (mRfxCas13d-NLS, blue), optimized 2C-NLS (mRfxCas13d-2C-NLS, orange), heitag (mRfxCas13d-hei, green), cmyc-2C-NLS (cmyc-mRfxCas13d-2C-NLS, purple) and bpNLS (mRfxCas13d-bpNLS, red) versions of *RfxCas13d* mRNA targeting pri-miR430 (gpri-miR430). Configuration of NLS signals in the different NLS versions are shown in **Extended Data Fig. 4A**. (n) total number of embryos is shown for each condition. The results are shown as the averages ± standard deviation of the mean of each phenotypic category from at least two independent experiments. χ^2 statistical test was performed to indicated comparisons.
- C)** Cumulative plot of the mRNA levels that are degraded by different pathways (maternal, zygotic and miR-430) through early zebrafish development and determined by Vejnar et al., 2019⁵⁰ and Medina-Muñoz et al., 2021⁴⁹ in control (Non-injected; gray line), and different pri-miR430 KD conditions using cytoplasmic (mRfxCas13d; pink line), NLS (mRfxCas13d-NLS; blue line) or optimized NLS (mRfxCas13d-2C-NLS; orange line) versions of RfxCas13d. Number of mRNA controlled by each pathway is shown (n). 203 random mRNAs degraded by maternal and zygotic pathways were selected and *p*-values and distances (D, maximal vertical distance between the compared distribution) were calculated using Kolmogorov-Smirnov tests.
- D)** Stacked barplots showing percentage of observed phenotypes at 48 hpf upon pri-miR-430 targeting using mRfxCas13d-2C-NLS with and without a rescue by a mature miR-430. (n) total number of embryos is shown for each condition. The results are shown as the averages ± standard deviation of the mean of each observed phenotype. 1 nL of the indicated concentration of mature miR430

duplexes was injected. χ^2 statistical tests were performed for indicated comparisons.

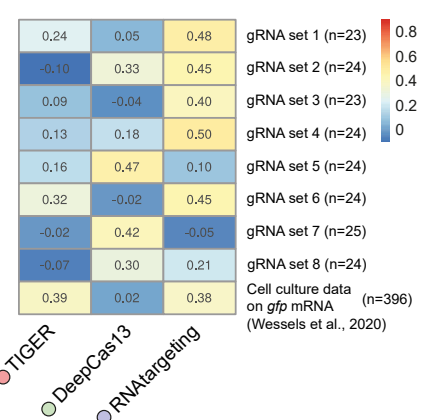
E) Barplots showing snRNA *u4atac* relative levels measured by qRT-PCR at 6 hpf comparing cytoplasmic (mRfxCas13d, pink), NLS (mRfxCas13d-NLS, blue) and optimized NLS (mRfxCas13d-2C-NLS, orange) versions of RfxCas13d. Results are shown as the averages \pm standard deviation of the mean from four biological replicates from two independent experiments. T-test statistical analyses were performed to compare control vs KD. miR-430b was used as a normalization control.

Moreno-Sánchez, Hernández-Huertas, Nahón-Cano et al. Fig. 4

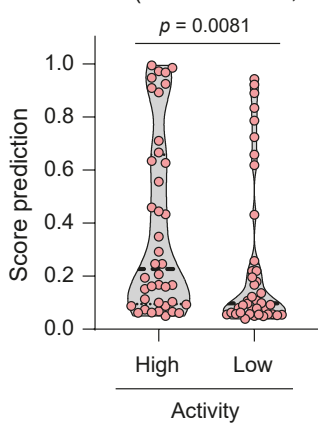
A



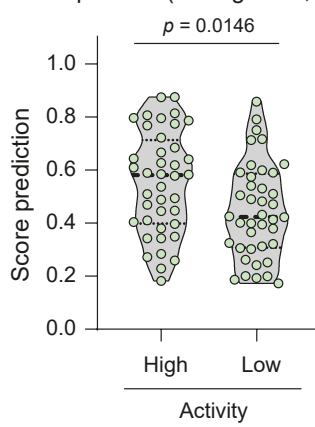
B R Pearson's correlations



C TIGER (Wessels et al., 2023)



D DeepCas13 (Cheng et al., 2023)



E RNAtargeting (Wei et al., 2023)

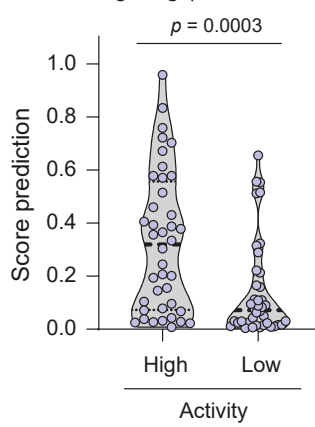


Figure 4. RNA-targeting, an ex vivo-based computational model can moderately predict CRISPR-RfxCas13d activity *in vivo*.

A) Workflow to assess the efficiency of computational models based on ex vivo data correlate to predict *in vivo* activity. 1) Diagram illustrating the injection of 8 different sets of 25 gRNAs together with RfxCas13d protein in one-cell stage zebrafish embryos. 2) RNAseq were performed from injected embryos at 4 hpf. Co-targeted mRNAs per set are depicted in red. 3) Fold Changes obtained from RNAseq data were used to calculate each gRNA efficiency and this employed to calculate Pearson correlation with scores obtained from the most recent and updated computational prediction models based on ex vivo data (Wessels et al., 2023¹⁷, Cheng et al., 2023¹⁸, Wei et al., 2023 Cell Systems¹⁹). See Methods for further details.

B) Heatmap of Pearson's correlations coefficient from each gRNA set with scores predicted by computational models in **A**: TIGER, red dots, Wessels et al., 2023¹⁷; DeepCas13, green dots, Cheng et al., 2023¹⁸; RNAtargeting, purple dots, Wei et al., 2023¹⁹). Pearson's correlations coefficient per computational model from cell culture data on *gfp* mRNA targeting using 396 gRNAs is included as a reference control (Wessels et al., 2020¹⁶).

C, D, E) Violin-plots representing the score of the five highest (High) and five lowest (Low) active gRNAs per set predicted by TIGER¹⁷ (**C**), DeepCas13¹⁸ (**D**) and RNAtargeting¹⁹ (**E**). The median and first and third quartiles of the 40 gRNAs score are represented as dashed and dotted lines, respectively. Non-parametric Mann-Whitney U statistical tests were performed to compare the score of high and low active gRNAs.

Moreno-Sánchez, Hernández-Huertas, Nahón-Cano et al. Fig. 5

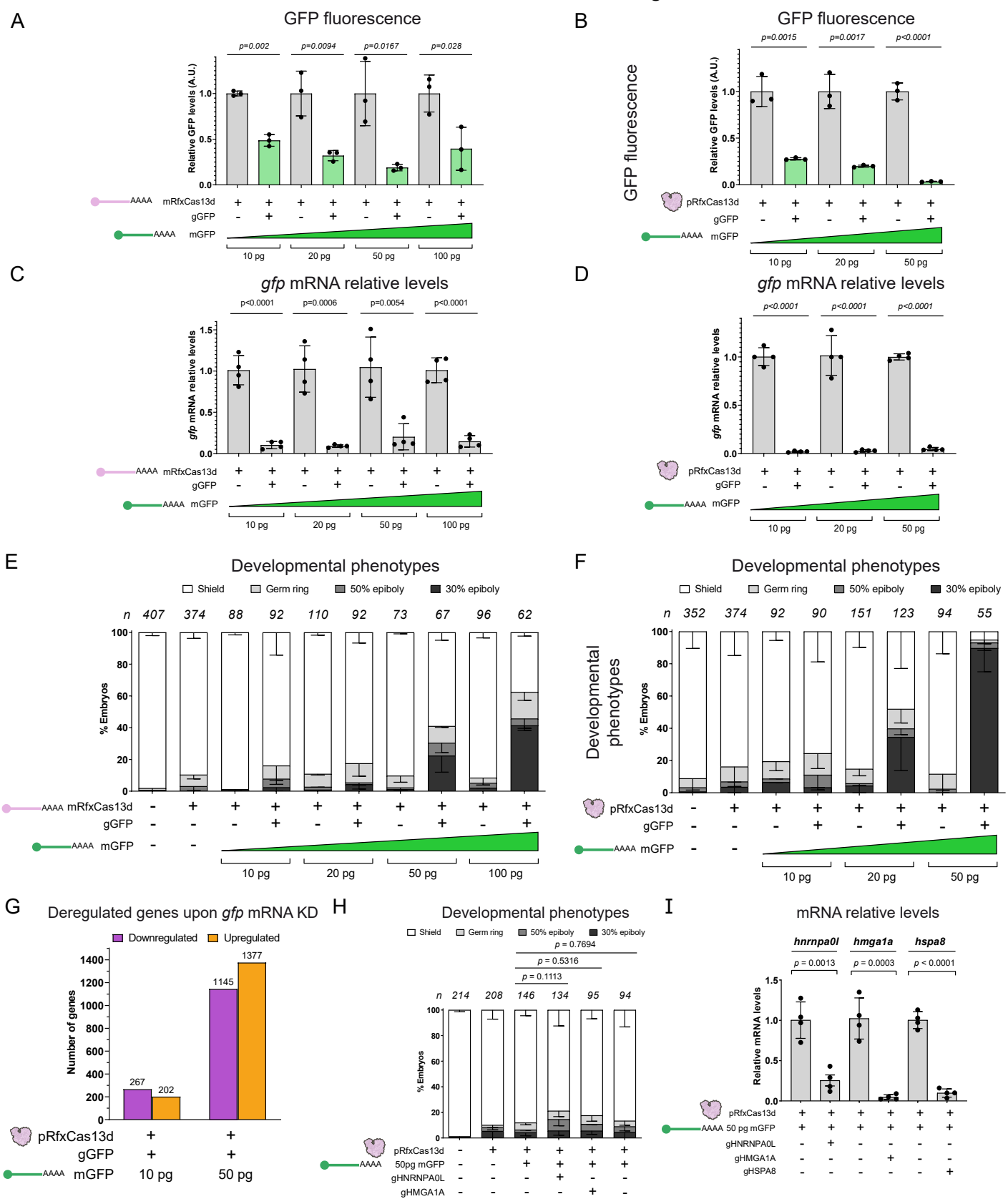


Figure 5. CRISPR-RfxCas13d exhibits physiologically relevant collateral activity only when targeting extremely abundant ectopic mRNAs in zebrafish embryos.

A, B) Barplots showing GFP fluorescence levels of injected embryos with RfxCas13d mRNA (mRfxCas13d, **A**) or RfxCas13d protein (pRfxCas13d, **B**) together with gRNAs (gGFP) targeting 10, 20, 50 or 100 pg of ectopic *gfp* mRNA (mGFP). Results are shown as the averages ± standard deviation of the mean from three biological replicates of 5 embryos each. T-test statistical analyses were performed, *p*-value is indicated above.

C, D) Barplots showing *gfp* mRNA relative levels analyzed by qPCR of injected embryos with mRfxCas13d (**C**) or pRfxCas13d (**D**) together with gGFP targeting 10, 20, 50 or 100 pg of ectopic mGFP. Results are shown as the averages ± standard deviation of the mean from four biological replicates from two independent experiments. T-test statistical analyses were performed, *p*-value is indicated above.

E, F) Stacked barplots representing developmental phenotypes (epiboly stages) of injected embryos with mRfxCas13d (**E**) or pRfxCas13d (**F**) together with gGFP targeting 10, 20, 50 or 100 pg of ectopic mGFP. Representative images of indicated epiboly stages are shown in **Fig. 1C**. (n) total number of embryos is displayed for each condition. The results are shown as the averages ± standard deviation of the mean of each developmental stage from at least two independent experiments.

G) Number of down- (purple) and up-regulated (orange) genes from injected embryos with pRfxCas13d together with gGFP and 10 or 50 pg of mGFP. Fold-Change of 2 and *p*-value < 0.001 were set to determine deregulated genes.

H) Stacked barplots representing developmental phenotypes (epiboly stages) of injected embryos with pRfxCas13d together with 50 pg of mGFP as reporter for collateral activity and gRNAs targeting endogenous *hnrmrp0l*, *hmga1a* and *hspa8* transcripts (gHNRNPA0L, gHMGA1A and gHSPA8, respectively). Representative images of indicated epiboly stages are shown in **Fig. 1C**. χ^2 statistical analyses were performed comparing side-by-side each KD condition with embryos injected with pRfxCas13d + mGFP. (n) total number of embryos is displayed for each condition. The results are shown as the averages ± standard

deviation of the mean of each developmental stage from at least two independent experiments.

I) Barplots showing mRNA relative levels analyzed by qRT-PCR at 6 hpf of injected embryos with pRfxCas13d together with 50 pg of mGFP as reporter for collateral activity and gHNRNPA0L, gHMGA1A or gHSPA8. Results are shown as the averages ± standard deviation of the mean from four biological replicates from two independent experiments. T-test statistical analyses were performed comparing side-by-side each KD condition with embryos injected with pRfxCas13d + mGFP. *taf15* mRNA was used as a normalization control.

Moreno-Sánchez, Hernández-Huertas, Nahón-Cano et al. Fig. 6

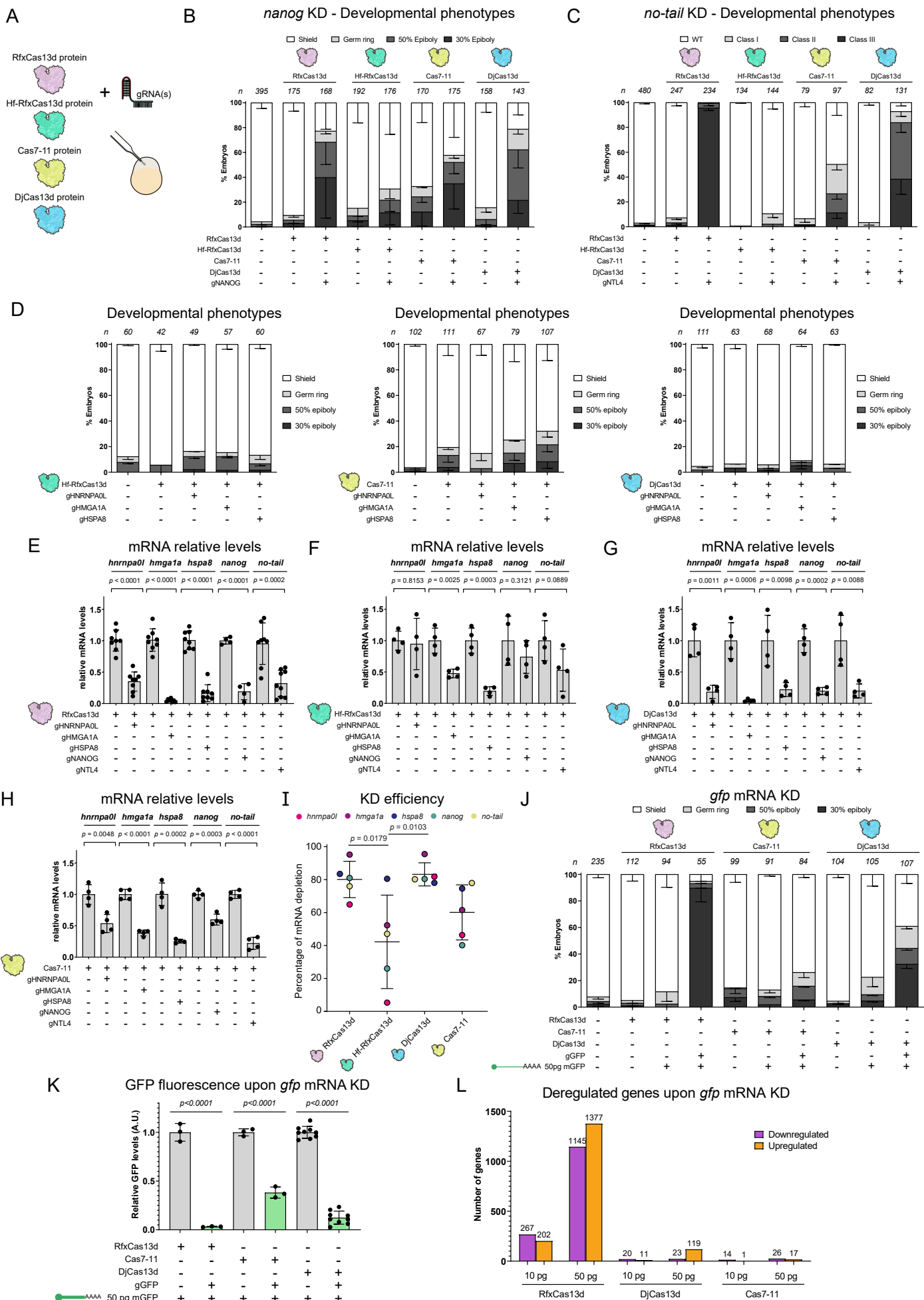


Figure 6. Implementation of alternative CRISPR-Cas systems for transient RNA-targeting *in vivo*.

- A)** Schematic illustration of the experimental setup used to compare alternative and high-fidelity CRISPR-Cas RNA targeting systems (Hf-RfxCas13d, DjCas13d and Cas7-11) with CRISPR-RfxCas13d. One-cell stage zebrafish embryos were injected with 3 ng of each purified protein together with 1 ng of a mix of three gRNAs (~300 from each gRNA).
- B, C)** Stacked barplots representing developmental phenotypes from injected embryos with RfxCas13d, Hf-RfxCas13d, Cas7-11 or DjCas13d together with three gRNAs targeting *nanog* (gNANOG, **B**) or one gRNA targeting *no-tail* (gNTL4, **C**). Representative images of epiboly stages and *no-tail* phenotypes are shown in **Fig. 1C**. (n) total number of embryos is shown for each condition. The results are shown as the averages ± standard deviation of the mean of each developmental stage from at least two independent experiments.
- D)** Stacked barplots representing developmental phenotypes (epiboly stages) of injected embryos with Hf-RfxCas13d, Cas7-11 or DjCas13d together with gRNAs targeting endogenous *hnrrnpa0l*, *hmga1a* and *hspa8* transcripts (gHNRNPA0L, gHMGA1A and gHSPA8, respectively). Representative images of epiboly stages are shown in **Fig. 1C**. (n) total number of embryos is displayed for each condition. The results are shown as the averages ± standard deviation of the mean of each developmental stage from at least two independent experiments.
- E, F, G, H)** Barplots showing mRNA relative levels analyzed by qRT-PCR at 4 or 6 hpf of injected embryos with RfxCas13d (**E**), Hf-RfxCas13d (**F**), DjCas13d (**G**) or Cas7-11 (**H**) together with gHNRNPA0L, gHMGA1A, gHSPA8, gNANOG or gNTL4. Results are shown as the averages ± standard deviation of the mean from at least four biological replicates from two or more independent experiments. T-test statistical analyses were performed comparing side-by-side each KD condition with embryos injected only with RfxCas13d, Hf-RfxCas13d, DjCas13d or Cas7-11. *hnrrnpa0l*, *hmga1a* and *hspa8* relative mRNA levels displayed in **Fig. 6E** correspond to **Fig. 5I** and **Extended Data Fig. 8F** data. *taf15* mRNA was used as a normalization control.
- I)** Dot-blot showing KD efficiency of RfxCas13d, Hf-RfxCas13d, Cas7-11 and DjCas13d. Each dot represents the mean of the percentage of mRNA depletion analyzed by qRT-PCR from **E-H** panels for the indicated mRNAs in colors; mean

and standard deviation are shown. One-way ANOVA followed by Tukey post-hoc analysis was performed, showing *p*-values only for comparisons with significant differences.

J) Stacked barplots representing developmental phenotypes (epiboly stages) of injected embryos with RfxCas13d, Cas7-11 or DjCas13d together with gRNAs targeting *gfp* (gGFP) and 50 pg of ectopic *gfp* mRNA (mGFP). Representative images of epiboly stages are shown in **Fig. 1C**. (n) total number of embryos is displayed for each condition. The results are shown as the averages ± standard deviation of the mean of each developmental stage from at least two independent experiments.

K) Barplots showing GFP fluorescence relative levels at 6 hpf of injected embryos with RfxCas13d, Cas7-11 or DjCas13d together with gGFP and 50 pg of ectopic mGFP. Results are shown as the averages ± standard deviation of the mean from at least three biological replicates of 5 embryos from two independent experiments. T-test statistical analyses were performed, *p*-value is indicated above.

L) Number of down- (purple) and up-regulated (orange) genes analyzed by RNAseq in injected embryos with RfxCas13d, DjCas13d or Cas7-11 together with gGFP and 10 or 50 pg of mGFP. Fold-Change of 2 and *p*-value < 0.001 were used to determine deregulated genes. Deregulated genes shown for RfxCas13d are from **Fig. 5G**.